

Time-integrated Optimal Transport: A Robust Minimax Framework

Thai P.D. Nguyen*

Hong T.M. Chu†

Kim-Chuan Toh‡

Abstract

Comparing time series in a principled manner requires capturing both temporal alignment and distributional similarity of features. Optimal transport (OT) has recently emerged as a powerful tool for this task, but existing OT-based approaches often depend on manually selected balancing parameters and can be computationally intensive. In this work, we introduce the Time-integrated Optimal Transport (TiOT) framework, which integrates temporal and feature components into a unified objective and yields a well-defined metric on the space of probability measures. This metric preserves fundamental properties of the Wasserstein distance, while avoiding the need for parameter tuning. To address the corresponding computational challenges, we introduce an entropic regularized approximation of TiOT, which can be efficiently solved using a block coordinate descent algorithm. Extensive experiments on both synthetic and real-world time series datasets demonstrate that our approach achieves improved accuracy and stability while maintaining comparable efficiency.

Keywords. Optimal transport, entropic regularization, time series, block coordinate descent.

MSC codes. 90C08, 90C47, 90C99, 65K05

1 Introduction

The Optimal Transport (OT) problem, whose history dates back to the seminal works of Monge (1781) [32] and Kantorovich (1942) [30], has long been a central tool in mathematical analysis and applications. At its core, it concerns the question of how to transport one distribution of mass into another with minimal costs. The ubiquity and versatility of this idea have led itself to links with many branches of mathematics and beyond. Many applications of optimal transport are based on the distance it induces (the Wasserstein distance \mathcal{W}_p), which possesses several fundamental properties, such as reproducing the structure of the underlying space in the space of probability measures and metrizing the weak convergence of probability measures. Equipped with these properties, the distance has been used to provide existence, stability, and uniqueness results of solutions of many important PDEs such as Euler flows [6], gradient flows [39, 29]. More broadly, this theoretical foundation has provided a rigorous basis for advances in diverse areas, including game theory, economics, statistics [39, 16], image processing and shape recognition [22, 24], and even physics [20].

*College of Engineering and Computer Science, VinUniversity (thai.npd@vinuni.edu.vn).

†(Corresponding author) College of Engineering and Computer Science, VinUniversity (hong.ctm@vinuni.edu.vn).

‡Department of Mathematics, and Institute of Operations Research and Analytics, National University of Singapore, Singapore 119076 (mattohkc@nus.edu.sg).

Recently, optimal transport has also found a natural role in modern machine learning, with applications in areas such as domain adaptation [9], computer graphics [5], and supervised learning [21]. Underlying these advances are several essential properties of OT. A prominent example is its ability to metrize weak convergence, which has proven crucial in the development of Wasserstein generative adversarial networks [1]. Another example is OT’s metric properties, which have been exploited to accelerate similarity search algorithms like the Approximating and Elimination Search Algorithm [31]. In parallel, the introduction of entropic regularization has greatly improved the scalability of OT in large-scale learning problems, giving rise to the Sinkhorn algorithm [10], which combines computational efficiency with a provable linear convergence rate [19, 7].

Among various data types studied in machine learning, time series play a particularly important role, appearing in healthcare [33], finance [43], economics [23], and industrial processes [8]. To analyze such data effectively, many machine learning algorithms rely on a well-defined notion of distance to measure the dissimilarity between samples. Dynamic Time Warping (DTW) [38] has long been regarded as a standard tool for this task. However, the absence of certain desirable properties for example the metric property in some cases yields unexpected inaccuracy [27]. Built on a more solid theoretical basis, the optimal transport problem has lately emerged as a viable alternative in comparing the dissimilarity between time series. In order to utilize the Wasserstein distance for time series, one needs to reasonably incorporate the temporal information into the problem. One possible approach is to impose additional time-dependent constraints on the classical OT problem [2, 15, 40]. Notably, Adapted Optimal Transport (AOT) [2, 15], which considers only bicausal couplings, can preserve several fundamental properties of the classical OT problem. Nonetheless, although this approach is conceptually natural, its empirical effectiveness has not yet been extensively demonstrated. From an orthogonal perspective, one could define the ground metric as a combination of temporal differences and differences in the other dimensions of the time series. This idea has been utilized in [42, 46]. Compared to AOT, the latter approach is simpler, easier to implement and has shown its promising empirical performance in [46]. However, a major disadvantage of this approach is the need for additional parameter tuning to balance the trade-off between the time dimension and other dimensions, which can be costly when dealing with large datasets.

Our contributions To address the aforementioned issues of the current OT-based methods for computing distance between time series, our work provides the following contributions:

- We propose the Time-integrated Optimal Transport problem (TiOT), a novel minimax framework that automatically balances temporal and feature information, thus eliminating the need for manual parameter tuning. In addition, we prove that TiOT induces a proper metric, denoted as \mathcal{D}_p , on the space of probability measures, and this metric retains key theoretical properties of the Wasserstein distance \mathcal{W}_p , such as metrizing weak convergence.
- We introduce an entropic regularized counterpart eTiOT as a fast and reliable approximation of the proposed TiOT problem, and, prove that its solutions converge to those of the original TiOT as the regularization parameter tends to zero.
- We develop a Block Coordinate Descent (BCD) algorithm to solve the eTiOT problem and analyze the convergence of this framework based on the theory of BSUM methods [37, 25]. Finally, we demonstrate the empirical effectiveness of the proposed metric \mathcal{D}_p and the

computational efficiency of the BCD algorithm through various numerical experiments, including classification tasks on real-world time series datasets.

Robust minimax optimal transport has been a subject of considerable study; see, e.g., [34, 14, 28, 13, 26], and references therein. Nevertheless, these studies do not address the incorporation of temporal information in time series within the optimal transport framework, a setting that, as we later demonstrate, admits strong theoretical guarantees and favorable empirical performance.

Structure of the paper We begin with notation and preliminaries. Section 2 introduces the formulations of TiOT and eTiOT and establishes key theoretical results. Section 3 develops a block coordinate descent algorithm for eTiOT and analyzes its convergence. Section 4 presents numerical experiments that validate our analysis and highlight the advantages of our framework in practical scenarios. Finally, Section 5 summarizes the main findings.

Notation We write $P(X)$ for the space of probability measures on X . For a measurable map $T : X \rightarrow Y$ and a measure $\alpha \in P(X)$, $T_{\#}\alpha$ denotes the pushforward of α through T , and Id is the identity map. The standard inner product on \mathbb{R}^d is denoted as $\langle x, y \rangle = \sum_{i=1}^d x_i y_i$ and its induced Euclidean norm is denoted as $\|x\|_2 = (\sum_{i=1}^d x_i^2)^{1/2}$. The i -th canonical basis vector of \mathbb{R}^d is denoted by $e_i = (0, \dots, 0, 1, 0, \dots, 0)^\top$, with 1 in the i -th position. The vector of all ones is denoted by $\mathbb{1}_d = (1, 1, \dots, 1)^\top \in \mathbb{R}^d$. Given a weight vector $a = (a_1, \dots, a_d)^\top$ with $a_i > 0$ and $\sum_{i=1}^d a_i = 1$, the weighted L^2 norm is $\|x\|_{L^2(a)} = (\sum_{i=1}^d a_i x_i^2)^{1/2}$. For vectors or matrices x, y , $x \circ y$ denotes their element-wise (Hadamard) product, and $x \oslash y$ their element-wise division. In this paper, which focuses on the analysis of time series data, we work with the underlying space \mathbb{R}^{d+1} , where the last coordinate explicitly represents time. The space of probability measures on (\mathbb{R}^{d+1}, d_p) with finite p -th moment is denoted as

$$P_p(\mathbb{R}^{d+1}) := \left\{ \mu \in P_p(\mathbb{R}^{d+1}) : \int_{\mathbb{R}^{d+1}} d_p(z_0, z)^p \mu(dz) < +\infty \right\},$$

where $z_0 \in \mathbb{R}^{d+1}$ is arbitrary, $d_p(z, z') = \|z - z'\|_p = \left(\sum_{i=1}^{d+1} |z_i - z'_i|^p \right)^{1/p}$.

We now recall the definition of the optimal transport problem and the associated Wasserstein distance, which serve as the starting point for our formulation of the Time-integrated Optimal Transport problem.

Definition 1.1. Given $\alpha, \beta \in P_p(\mathbb{R}^{d+1})$, and $c : \mathbb{R}^{d+1} \times \mathbb{R}^{d+1} \rightarrow [0, +\infty]$, the Optimal Transport problem (OT) is formulated as follows

$$\inf \left\{ \int_{\mathbb{R}^{d+1} \times \mathbb{R}^{d+1}} c(z, z') d\pi(z, z') : \pi \in \Pi(\alpha, \beta) \right\}, \quad (1)$$

where $\Pi(\alpha, \beta) = \{ \pi \in P(\mathbb{R}^{d+1} \times \mathbb{R}^{d+1}) : \pi(A \times \mathbb{R}^{d+1}) = \alpha(A), \pi(\mathbb{R}^{d+1} \times B) = \beta(B) \}$ for any measurable subsets $A, B \subset \mathbb{R}^{d+1}$.

One might regard the optimal value of the OT problem as a way to measure the discrepancy between two measures. In general, it does not satisfy the axioms of distance, but if the probability measures are restricted to the set $P_p(\mathbb{R}^{d+1})$ and the metric d_p is used to construct the cost function, then the formulation (1) induces a proper distance, generally known as the Wasserstein distance.

Definition 1.2. Let $p \in [1, \infty)$ and two probability measures α, β in $P_p(\mathbb{R}^{d+1})$. The Wasserstein distance of order p between α and β is defined as follows:

$$\mathcal{W}_p(\alpha, \beta) = \left(\min_{\pi \in \Pi(\alpha, \beta)} \int_{\mathbb{R}^{d+1} \times \mathbb{R}^{d+1}} d_p(z, z')^p d\pi(z, z') \right)^{1/p}. \quad (2)$$

We conclude this section by recalling the common notion of convergence for probability measures, namely weak convergence in $P_p(\mathbb{R}^{d+1})$.

Definition 1.3 (Weak convergence in $P_p(\mathbb{R}^{d+1})$). Given $p \in [1, \infty)$, let $(\mu_k)_{k \in \mathbb{N}}$ be a sequence of probability measures in $P_p(\mathbb{R}^{d+1})$ and let μ be another element of $P_p(\mathbb{R}^{d+1})$. Then (μ_k) is said to converge weakly in $P_p(\mathbb{R}^{d+1})$ if for any bounded continuous function ϕ and $z_0 \in \mathbb{R}^{d+1}$:

$$\int \phi d\mu_k \rightarrow \int \phi d\mu \quad \text{and} \quad \int d_p(z_0, z)^p d\mu_k(z) \rightarrow \int d_p(z_0, z)^p d\mu(z).$$

2 Time-integrated Optimal Transport

To address the limitations of current OT-based metrics for time series [2, 15, 40, 46, 42], we introduce the Time-integrated Optimal Transport problem (TiOT), which explicitly incorporates temporal information into the OT cost matrix. The guiding principle of TiOT is to reformulate the optimal transport problem in a way that achieves the maximum discrimination between two time series. Ideally, this expansion should not be uniform across all pairs of time series: it should be weaker for series that are intrinsically closer to each other and stronger for those that are intrinsically more distant. The formal formulation of this idea is given below, while its numerical advantages will be elaborated in later experiments.

Definition 2.1 (Time-integrated Optimal Transport). Given $\alpha, \beta \in P_p(\mathbb{R}^{d+1})$, the Time-integrated Optimal Transport problem between these measures reads

$$\begin{aligned} \mathcal{D}_p(\alpha, \beta) &= \max_{w \in [0, 1]} \left[\min_{\pi \in \Pi(\alpha, \beta)} \int_{\mathbb{R}^{d+1} \times \mathbb{R}^{d+1}} d_{p,w}((x, t), (y, s))^p d\pi((x, t), (y, s)) \right]^{1/p} \\ &= \max_{w \in [0, 1]} \mathcal{W}_{p,w}(\alpha, \beta), \end{aligned} \quad (3)$$

where $p \geq 1$ and $d_{p,w}((x, t), (y, s)) = (w\|x - y\|_p^p + (1 - w)|t - s|^p)^{1/p}$. In particular, $d_p = 2^{1/p} \times d_{p,1/2}$ and $\mathcal{W}_p = 2^{1/p} \times \mathcal{W}_{p,1/2}$.

Remark 2.2. We give some remarks on the TiOT problem:

- For $\alpha, \beta \in P_p(\mathbb{R}^{d+1})$, the function $d_{p,w}^p$ is integrable with respect to any coupling π , since d_p^p is integrable with respect to π and $d_{p,w}(z, z') \leq d_p(z, z')$ for all $z, z' \in \mathbb{R}^{d+1}$ and $w \in [0, 1]$. Thus, the finiteness of \mathcal{D}_p is guaranteed.
- In general, $d_{p,w}$ is only a pseudometric, as the positivity axiom may fail when $w = 0$ or $w = 1$. Nevertheless, we will later show that this is sufficient for $(P_p(\mathbb{R}^{d+1}), \mathcal{D}_p)$ to form a metric space, as a result of the maximum property.
- The existence of an optimal solution of (3) is given in Appendix A.

In the following sections, we use the notation $\mathcal{W}_{p,w}$ to denote the p -Wasserstein distance with respect to the underlying metric $d_{p,w}$, and \mathcal{W}_p to denote the ordinary p -Wasserstein distance with the standard metric d_p defined in (2).

2.1 Time-integrated Optimal Transport metric space

In this section, we show that \mathcal{D}_p is a natural extension of the classical Wasserstein distance \mathcal{W}_p , in the sense that \mathcal{D}_p preserves several fundamental properties of \mathcal{W}_p . We begin by demonstrating that \mathcal{D}_p satisfies the metric property, which is essential for any distance function. We then extend various convergence and topological characterizations from $(P_p(\mathbb{R}^{d+1}), \mathcal{W}_p)$ to $(P_p(\mathbb{R}^{d+1}), \mathcal{D}_p)$.

Theorem 2.3. *The Time-integrated Optimal Transport function \mathcal{D}_p is a distance on $P_p(\mathbb{R}^{d+1})$.*

Proof. We now verify, in sequence, the symmetry, positivity, and triangle inequality for \mathcal{D}_p . Let $\alpha, \beta \in P_p(\mathbb{R}^{d+1})$ with supports X, Y . First, we have $\mathcal{D}_p(\alpha, \beta) = \mathcal{D}_p(\beta, \alpha)$ by the symmetry of $d_{p,w}$.

Second, to show $\mathcal{D}_p(\alpha, \alpha) = 0$, consider the diagonal coupling $\pi_0 := (\text{Id} \times \text{Id})_{\#}\alpha$, that is, $\pi_0(V) = \alpha(\{(x, t) : ((x, t), (x, t)) \in V\})$ for any measurable $V \subset X \times X$. Then $\pi_0 \in \Pi(\alpha, \alpha)$ and $d_{p,w}((x, t), (x, t)) = 0$ for all $w \in [0, 1]$. Therefore, for any $w \in [0, 1]$

$$\begin{aligned} \mathcal{W}_{p,w}(\alpha, \alpha) &= \min_{\pi \in \Pi(\alpha, \alpha)} \int_{X \times X} d_{p,w}((x, t), (y, s))^p d\pi((x, t), (y, s)) \\ &\leq \int_{X \times X} d_{p,w}((x, t), (y, s))^p d\pi_0((x, t), (y, s)) = 0. \end{aligned}$$

Hence, by definition, $\mathcal{D}_p(\alpha, \alpha) = \max_{w \in [0, 1]} \mathcal{W}_{p,w}(\alpha, \alpha) = 0$. If $\mathcal{D}_p(\alpha, \beta) = 0$, then for any $w \in [0, 1]$, $\mathcal{W}_{p,w}(\alpha, \beta) \leq \mathcal{D}_p(\alpha, \beta) = 0$. Thus, $\mathcal{W}_{p,w}(\alpha, \beta) = 0$ for all $w \in [0, 1]$. Since $\mathcal{W}_{p,w}$ is a valid metric for $w \in (0, 1)$, it follows that $\alpha = \beta$.

Third, to prove the triangle inequality, we invoke the Gluing Lemma [44]. Let $\xi \in P_p(\mathbb{R}^{d+1})$ be supported on Z , and let π_{xy}^*, π_{yz}^* be optimal couplings for (α, β) and (β, ξ) , respectively. The lemma ensures the existence of $\pi \in P(X \times Y \times Z)$ with marginals $\pi_{xy} = \pi_{xy}^*$ and $\pi_{yz} = \pi_{yz}^*$. Its marginal π_{xz} then belongs to $\Pi(\alpha, \xi)$. Hence,

$$\begin{aligned} \mathcal{D}_p(\alpha, \xi) &\leq \max_{w \in [0, 1]} \left[\int_{X \times Z} d_{p,w}((x, t), (z, e))^p d\pi_{xz} \right]^{1/p} \\ &= \max_{w \in [0, 1]} \left[\int_{X \times Y \times Z} d_{p,w}((x, t), (z, e))^p d\pi \right]^{1/p} \\ &\leq \max_{w \in [0, 1]} \left[\int_{X \times Y \times Z} (d_{p,w}((x, t), (y, s)) + d_{p,w}((y, s), (z, e)))^p d\pi \right]^{1/p}, \end{aligned} \tag{4}$$

where the first inequality comes from the feasibility of π_{xz} , and the second from the triangle inequality for $d_{p,w}$ (a direct consequence of the L_p norm triangle inequality). Next, we bound the right-hand side (RHS) of (4)

$$\begin{aligned} \text{RHS of (4)} &\leq \max_{w \in [0, 1]} \left\{ \left[\int_{X \times Y \times Z} d_{p,w}((x, t), (y, s))^p d\pi \right]^{1/p} \right. \\ &\quad \left. + \left[\int_{X \times Y \times Z} d_{p,w}((y, s), (z, e))^p d\pi \right]^{1/p} \right\} \\ &= \max_{w \in [0, 1]} \left\{ \left[\int_{X \times Y} d_{p,w}((x, t), (y, s))^p d\pi_{xy}^* \right]^{1/p} \right. \\ &\quad \left. + \left[\int_{Y \times Z} d_{p,w}((y, s), (z, e))^p d\pi_{yz}^* \right]^{1/p} \right\} \\ &\leq \max_{w \in [0, 1]} \left[\int_{X \times Y} d_{p,w}((x, t), (y, s))^p d\pi_{xy}^* \right]^{1/p} \\ &\quad + \max_{w \in [0, 1]} \left[\int_{Y \times Z} d_{p,w}((y, s), (z, e))^p d\pi_{yz}^* \right]^{1/p} \\ &= \mathcal{D}_p(\alpha, \beta) + \mathcal{D}_p(\beta, \xi). \end{aligned}$$

Here the first inequality follows from the Minkowski inequality and the last inequality from the property of the max function. This completes the proof. \square

The following proposition establishes that \mathcal{D}_p is equivalent to the classical \mathcal{W}_p distance. This result is crucial, as it enables the natural extension of convergence and topological properties from $(P_p(\mathbb{R}^{d+1}), \mathcal{W}_p)$ to $(P_p(\mathbb{R}^{d+1}), \mathcal{D}_p)$. Ensuring these properties is essential and has been shown to play a significant role in various theoretical and applied contexts [6, 39, 29, 1].

Proposition 2.4. *Given $p \in [1, \infty)$, we have*

$$\left(\frac{1}{2}\right)^{1/p} \mathcal{W}_p \leq \mathcal{D}_p \leq \mathcal{W}_p. \quad (5)$$

Proof. We begin by proving the first inequality. By the definition of \mathcal{D}_p we have that for any $w \in [0, 1]$, $\mathcal{D}_p \geq \mathcal{W}_{p,w}$. Choose $w = \frac{1}{2}$, we obtain for any $\alpha, \beta \in P_p(\mathbb{R}^{d+1})$,

$$\begin{aligned} \mathcal{D}_p(\alpha, \beta) &\geq \min_{\pi \in \Pi(\alpha, \beta)} \left(\int_{\mathbb{R}^{d+1} \times \mathbb{R}^{d+1}} d_{p,1/2}((x, t), (y, s))^p d\pi \right)^{1/p} \\ &= \min_{\pi \in \Pi(\alpha, \beta)} \left(\int_{\mathbb{R}^{d+1} \times \mathbb{R}^{d+1}} \frac{1}{2} d_p((x, t), (y, s))^p d\pi \right)^{1/p} = \left(\frac{1}{2}\right)^{1/p} \mathcal{W}_p(\alpha, \beta). \end{aligned}$$

Thus the first inequality is established. The relation $d_{p,w} \leq d_p$ for all $w \in [0, 1]$ then yields the second inequality immediately. \square

Corollary 1. *Given $p \in [1, \infty)$ and let $(\mu_k)_{k \in \mathbb{N}}$ be a Cauchy sequence in $(P_p(\mathbb{R}^{d+1}), \mathcal{D}_p)$. Then $\{\mu_k\}$ is tight.*

Proof. By the first inequality of (5), if a sequence is a Cauchy sequence in $(P_p(\mathbb{R}^{d+1}), \mathcal{D}_p)$ then it must also be a Cauchy sequence in $(P_p(\mathbb{R}^{d+1}), \mathcal{W}_p)$. Combine with the classical result that Cauchy sequences in \mathcal{W}_p sense are tight [45, Lemma 6.14], the proof is completed. \square

We recall that a natural notion of convergence for measures in $P_p(\mathbb{R}^{d+1})$ is weak convergence (definition 1.3). It is known to be equivalent to convergence induced by the metric \mathcal{W}_p , and, by the bounds in (5), we could show that the same property holds for \mathcal{D}_p .

Theorem 2.5 (convergence in \mathcal{D}_p). *If $(\mu_k)_{k \in \mathbb{N}}$ is a sequence of measures in $P_p(\mathbb{R}^{d+1})$ and μ is another measure in $P(\mathbb{R}^{d+1})$, then the following two statements are equivalent:*

(i) μ_k converges weakly in $P_p(\mathbb{R}^{d+1})$ to μ ;

(ii) $\mathcal{D}_p(\mu_k, \mu) \rightarrow 0$.

Proof. Assume that $\mu_k \rightharpoonup \mu$, by [45, Theorem 6.9], we have $\mathcal{W}_p(\mu_k, \mu) \rightarrow 0$. Since $\mathcal{D}_p \leq \mathcal{W}_p$ by the bound in proposition 2.4, we have $\mathcal{D}_p(\mu_k, \mu) \rightarrow 0$ as μ_k converges weakly to μ .

Conversely, suppose $\mathcal{D}_p(\mu_k, \mu) \rightarrow 0$. Then $0 \leq \left(\frac{1}{2}\right)^{1/p} \mathcal{W}_p \leq \mathcal{D}_p$ in proposition 2.4 implies that $\mathcal{W}_p(\mu_k, \mu) \rightarrow 0$. Hence it follows from [45, Theorem 6.9] that μ_k converges weakly to μ in $P_p(\mathbb{R}^{d+1})$. \square

Corollary 2 (continuity of \mathcal{D}_p). *Given $p \in [1, \infty)$, \mathcal{D}_p is continuous on $P_p(\mathbb{R}^{d+1})$. To be specific, if μ_k (resp. ν_k) converges to μ (resp. ν) weakly in $P_p(\mathbb{R}^{d+1})$ as $k \rightarrow \infty$, then*

$$\mathcal{D}_p(\mu_k, \nu_k) \rightarrow \mathcal{D}_p(\mu, \nu).$$

The corollary on the continuity of \mathcal{D}_p above is a direct consequence of Theorem 2.5 and the triangle inequality of \mathcal{D}_p . Next we show that $(P_p(\mathbb{R}^{d+1}), \mathcal{D}_p)$ preserves the polish property of the base space \mathbb{R}^{d+1} just like the Wasserstein distance.

Theorem 2.6 (topology of \mathcal{D}_p space). *The space $P_p(\mathbb{R}^{d+1})$ equipped with the TiOT distance \mathcal{D}_p is a complete separable metric space.*

Proof. Since $(P_p(\mathbb{R}^{d+1}), \mathcal{W}_p)$ is a separable space, there exists a countable dense set $\mathcal{P} \in P_p(\mathbb{R}^{d+1})$ such that for any $\varepsilon > 0$ and $\mu \in P_p(\mathbb{R}^{d+1})$, there exists $\nu \in \mathcal{P}$ such that $\mathcal{W}_p(\mu, \nu) \leq \varepsilon$. By (5), we have $\mathcal{D}_p(\mu, \nu) \leq \mathcal{W}_p(\mu, \nu) \leq \varepsilon$. Therefore \mathcal{P} is also dense in $(P_p(\mathbb{R}^{d+1}), \mathcal{D}_p)$, thus, $(P_p(\mathbb{R}^{d+1}), \mathcal{D}_p)$ is separable.

The completeness of $P_p(\mathbb{R}^{d+1})$ with \mathcal{D}_p distance is again a direct consequence of the completeness of $P_p(\mathbb{R}^{d+1})$ with \mathcal{W}_p distance. In fact, let $(\mu_k)_{k \in \mathbb{N}}$ be a Cauchy sequence in $(P_p(\mathbb{R}^{d+1}), \mathcal{D}_p)$. Since $(\frac{1}{2})^{1/p} \mathcal{W}_p \leq \mathcal{D}_p$ (by the first bound in (5)), so $(\mu_k)_{k \in \mathbb{N}}$ is also a Cauchy sequence in $(P_p(\mathbb{R}^{d+1}), \mathcal{W}_p)$. Hence, Theorem 6.18 in [45] gives us the convergence of (μ_k) in \mathcal{W}_p sense, which leads to the convergence in \mathcal{D}_p sense by the second bound in (5). \square

We now turn to the computational aspects of the TiOT problem. For discrete measures, the TiOT problem reduces to a max–min problem of a bilinear function. By replacing the inner minimization by its dual, this problem can be reformulated as a linear program. The explicit formulation is provided in Appendix G.

Definition 2.7 (TiOT). The discrete TiOT problem between two discrete measures $\alpha = \sum_{i=1}^m a_i \delta_{(x_i, t_i)}$ and $\beta = \sum_{j=1}^n b_j \delta_{(y_j, s_j)}$ with $x_i, y_j \in \mathbb{R}^d$ is given by

$$\max_{w \in [0,1]} \min_{\pi \in \Pi(\alpha, \beta)} \langle C(w), \pi \rangle, \quad (6)$$

where $c_{i,j}(w) = w\|x_i - y_j\|_p^p + (1-w)|t_i - s_j|^p$ for $w \in [0, 1]$, and $\Pi(\alpha, \beta) = \{\pi \in \mathbb{R}_+^{m \times n} : \pi \mathbb{1}_n = a, \pi^\top \mathbb{1}_m = b\}$.

2.2 Entropic regularized Time-integrated Optimal Transport

Analogous to the entropic optimal transport, we introduce the entropic regularized Time-integrated Optimal Transport (eTiOT) problem by adding a Kullback–Leibler regularization term to the objective of the TiOT problem (6). This term, equivalent to the entropy function $\langle \pi, \log(\pi) \rangle$, is strictly convex and pushes the optimal solution into the interior of the feasible set, thereby simplifying the non-negativity constraint and favoring solutions closer to the independent coupling $\pi = a \circ b$. We show that eTiOT provides a reliable approximation of TiOT while offering substantial computational advantages, as will be demonstrated in Section 4.

Definition 2.8 (eTiOT). Let $\alpha = \sum_{i=1}^m a_i \delta_{(x_i, t_i)}$, $\beta = \sum_{j=1}^n b_j \delta_{(y_j, s_j)}$ be two discrete measures with $x_i, y_j \in \mathbb{R}^d$. The formulation of the entropic regularized Time-integrated Optimal Transport problem between them is as follows:

$$\max_{w \in [0,1]} \min_{\pi \in \Pi(\alpha, \beta)} \langle C(w), \pi \rangle + \varepsilon \mathbf{KL}(\pi | a \circ b), \quad (7)$$

where $c_{i,j}(w) = w\|x_i - y_j\|_p^p + (1-w)|t_i - s_j|^p$ for $w \in [0, 1]$, $\Pi(\alpha, \beta) = \{\pi \in \mathbb{R}_+^{m \times n} : \pi \mathbb{1}_n = a, \pi^\top \mathbb{1}_m = b\}$, and $\mathbf{KL}(\pi | \gamma) = \sum_{i,j} \pi_{ij} \log(\frac{\pi_{ij}}{\gamma_{ij}}) - \pi_{ij} + \gamma_{ij}$.

Before presenting an efficient algorithm for solving eTiOT in Section 3, we demonstrate that eTiOT is a proper surrogate for the original TiOT problem: as the regularization parameter ϵ decreases to zero, the solution of eTiOT converges to a solution of TiOT. While this is a standard result in classical optimal transport, (see [35, Proposition 4.1]), the extension to our framework is not straightforward. The challenges arise from the max-min structure in TiOT.

Theorem 2.9 (convergence with respect to ϵ). *Consider a positive sequence $\{\epsilon_k\}$. We denote $(w_k, \pi_{w_k}^{\epsilon_k})$ as the solution of the eTiOT problem with $\epsilon = \epsilon_k$ and \mathcal{S}^* as the set of optimal solutions of the TiOT problem. Then the following statements hold.*

- (i) *If $\epsilon_k \xrightarrow{k \rightarrow \infty} 0$, there exists a subsequence of $\{(w_k, \pi_{w_k}^{\epsilon_k})\}$ that converges to a point in \mathcal{S}^* .*
- (ii) *If $\epsilon_k \xrightarrow{k \rightarrow \infty} \infty$, the whole sequence $\pi_{w_k}^{\epsilon_k} \xrightarrow{k \rightarrow \infty} ab^\top$.*

Proof. (i) For a fixed value of $w \in [0, 1]$, we denote

$$\pi_w = \arg \min_{\pi \in \Pi(\alpha, \beta)} \langle C(w), \pi \rangle, \quad \pi_w^\epsilon = \arg \min_{\pi \in \Pi(\alpha, \beta)} \langle C(w), \pi \rangle + \epsilon \mathbf{KL}(\pi | \cdot),$$

where, for brevity, we write $\mathbf{KL}(\pi | \cdot)$ to mean $\mathbf{KL}(\pi | a \circ b)$.

Since $[0, 1], \Pi(\alpha, \beta)$ are compact, we can extract a subsequence such that (for the sake of simplicity, we keep the same notation) $\{w_k, \pi_{w_k}^{\epsilon_k}\} \rightarrow (\hat{w}, \hat{\pi})$ and $\hat{w} \in [0, 1]$, $\hat{\pi} \in \Pi(\alpha, \beta)$. Consider an arbitrary optimal solution of the TiOT problem (w^*, π_{w^*}) .

By the optimality of (w^*, π_{w^*}) we have

$$\langle C(w), \pi_w \rangle \leq \langle C(w^*), \pi_{w^*} \rangle \leq \langle C(w^*), \pi \rangle \quad \forall \pi \in \Pi(\alpha, \beta), w \in [0, 1], \quad (8)$$

where the first inequality stems from the property that for any $w \in [0, 1]$,

$$\langle C(w), \pi_w \rangle = \min_{\pi \in \Pi(\alpha, \beta)} \langle C(w), \pi \rangle \leq \max_{w \in [0, 1]} \min_{\pi \in \Pi(\alpha, \beta)} \langle C(w), \pi \rangle = \langle C(w^*), \pi_{w^*} \rangle,$$

and the second inequality follows from the property that for all $\pi \in \Pi(\alpha, \beta)$,

$$\langle C(w^*), \pi_{w^*} \rangle = \max_{w \in [0, 1]} \min_{\pi \in \Pi(\alpha, \beta)} \langle C(w), \pi \rangle = \min_{\pi \in \Pi(\alpha, \beta)} \langle C(w^*), \pi \rangle \leq \langle C(w^*), \pi \rangle.$$

In particular, when setting $w = w_k, \pi = \pi_{w_k}^{\epsilon_k}$ in (8), we get

$$\langle C(w_k), \pi_{w_k} \rangle \leq \langle C(w^*), \pi_{w^*} \rangle \leq \langle C(w^*), \pi_{w^*}^{\epsilon_k} \rangle. \quad (9)$$

Similarly, the optimality of $(w_k, \pi_{w_k}^{\epsilon_k})$ ensures that for any $w \in [0, 1]$ and $\pi \in \Pi(\alpha, \beta)$

$$\langle C(w), \pi_w^{\epsilon_k} \rangle + \epsilon_k \mathbf{KL}(\pi_w^{\epsilon_k} | \cdot) \leq \langle C(w_k), \pi_{w_k}^{\epsilon_k} \rangle + \epsilon_k \mathbf{KL}(\pi_{w_k}^{\epsilon_k} | \cdot) \leq \langle C(w_k), \pi \rangle + \epsilon_k \mathbf{KL}(\pi | \cdot). \quad (10)$$

Setting $w = w^*, \pi = \pi_{w_k}$ in (10), we get

$$\langle C(w^*), \pi_{w^*}^{\epsilon_k} \rangle + \epsilon_k \mathbf{KL}(\pi_{w^*}^{\epsilon_k} | \cdot) \leq \langle C(w_k), \pi_{w_k}^{\epsilon_k} \rangle + \epsilon_k \mathbf{KL}(\pi_{w_k}^{\epsilon_k} | \cdot) \leq \langle C(w_k), \pi_{w_k} \rangle + \epsilon_k \mathbf{KL}(\pi_{w_k} | \cdot). \quad (11)$$

From (11) and (9), we have

$$\begin{aligned} & \epsilon_k (\mathbf{KL}(\pi_{w^*}^{\epsilon_k} | \cdot) - \mathbf{KL}(\pi_{w_k}^{\epsilon_k} | \cdot)) \\ & \leq \langle C(w_k), \pi_{w_k}^{\epsilon_k} \rangle - \langle C(w^*), \pi_{w^*}^{\epsilon_k} \rangle \leq \langle C(w_k), \pi_{w_k}^{\epsilon_k} \rangle - \langle C(w^*), \pi_{w^*} \rangle \\ & \leq \langle C(w_k), \pi_{w_k}^{\epsilon_k} \rangle - \langle C(w_k), \pi_{w_k} \rangle \leq \epsilon_k (\mathbf{KL}(\pi_{w_k} | \cdot) - \mathbf{KL}(\pi_{w_k}^{\epsilon_k} | \cdot)). \end{aligned} \quad (12)$$

Since $\mathbf{KL}(\pi|\cdot)$ is a continuous function of π and $\Pi(\alpha, \beta)$ is compact, $\mathbf{KL}(\pi_{w_k}^{\varepsilon_k}|\cdot)$ and $\mathbf{KL}(\pi_{w_k}|\cdot)$ are both bounded. Thus as $\varepsilon_k \rightarrow 0$, by applying the squeeze theorem to (12), we get $\lim_{k \rightarrow \infty} \langle C(w_k), \pi_{w_k}^{\varepsilon_k} \rangle = \langle C(w^*), \pi_{w^*} \rangle$, so $\langle C(\widehat{w}), \widehat{\pi} \rangle = \langle C(w^*), \pi_{w^*} \rangle$. Therefore, by (8), we have

$$\langle C(w), \pi_w \rangle \leq \langle C(\widehat{w}), \widehat{\pi} \rangle, \quad \forall w \in [0, 1]. \quad (13)$$

Taking the limit as $\varepsilon_k \rightarrow 0$ in the second inequality of (10), we get

$$\langle C(\widehat{w}), \widehat{\pi} \rangle \leq \langle C(\widehat{w}), \pi \rangle, \quad \forall \pi \in \Pi(\alpha, \beta). \quad (14)$$

Combining (13) and (14), we have

$$\langle C(w), \pi_w \rangle \leq \langle C(\widehat{w}), \widehat{\pi} \rangle \leq \langle C(\widehat{w}), \pi \rangle, \quad \forall w \in [0, 1], \pi \in \Pi(\alpha, \beta), \quad (15)$$

which yields the optimality of $(\widehat{w}, \widehat{\pi})$ for problem TiOT. Hence $(\widehat{w}, \widehat{\pi}) \in \mathcal{S}^*$.

(ii) Similar to the above proof, take the sequence $\{\varepsilon_k\}$ that tends to $+\infty$ as $k \rightarrow \infty$, we have a subsequence $\{w_k, \pi_{w_k}^{\varepsilon_k}\} \rightarrow (\widehat{w}, \widehat{\pi})$ with $\widehat{w} \in [0, 1]$, $\widehat{\pi} \in \Pi(\alpha, \beta)$. Using the second inequality of (10) with $\pi = a \circ b$, we have

$$\langle C(w_k), \pi_{w_k}^{\varepsilon_k} \rangle + \varepsilon_k \mathbf{KL}(\pi_{w_k}^{\varepsilon_k} | a \circ b) \leq \langle C(w_k), a \circ b \rangle + \varepsilon_k \times 0,$$

which implies that

$$\varepsilon_k \mathbf{KL}(\pi_{w_k}^{\varepsilon_k} | a \circ b) \leq \langle C(w_k), a \circ b \rangle \leq \sum_{i,j} |C(w)_{ij}| a_i b_j \leq \|C(w)\|_{\infty} \sum_{i,j} a_i b_j \leq \|C\|_{\infty},$$

where $\|C\|_{\infty} = \max_{w \in [0,1]} \{\|C(w)\|_{\infty}\}$, and $\|C(w)\|_{\infty}$ is the maximum absolute value among all the entries of $C(w)$. Dividing both sides by ε_k and letting this value tends to ∞ , we get

$$\mathbf{KL}(\pi_{w_k}^{\varepsilon_k} | a \circ b) \rightarrow 0.$$

Thus, by the Pinsker's inequality [36], $\pi_{w_k}^{\varepsilon_k} \rightarrow a \circ b$. Then, the compactness of $\Pi(\alpha, \beta)$ ensures the convergence to $a \circ b$ of the whole sequence. \square

3 Block coordinate descent algorithm for solving eTiOT

One of the key developments that has substantially advanced the field of optimal transport is the introduction of its entropic regularized formulation [10, 4]. The Sinkhorn algorithm provides an efficient method for solving this problem, thereby enabling the application of optimal transport to large-scale machine learning tasks.

Indeed, the Sinkhorn algorithm can be interpreted as a block coordinate descent method applied to the dual formulation of the entropic OT problem. Motivated by this perspective, in this section we introduce a block coordinate descent algorithm for the eTiOT problem and establish its convergence under the natural normalization proposed in [7].

The Lagrangian of the inner minimization problem is given by

$$\mathbb{L}(\pi, u, v) = \langle \pi, C(w) \rangle + \varepsilon \mathbf{KL}(\pi | a \circ b) + u^T(a - \pi \mathbb{1}_n) + v^T(b - \pi^T \mathbb{1}_m).$$

Setting its gradient $\frac{\partial \mathbb{L}}{\partial \pi_{ij}} = C_{ij}(w) + \varepsilon \log\left(\frac{\pi_{ij}}{a_i b_j}\right) - u_i - v_j = 0$, we get

$$\pi_{ij} = a_i b_j \exp\left(\frac{u_i + v_j - c_{ij}(w)}{\varepsilon}\right) \quad \forall i \in [m], j \in [n].$$

Combining with the normalization in [7], the eTiOT problem is now given by

$$\min_{\substack{w \in [0,1], \\ u \in \mathbb{R}_a^m, v \in \mathbb{R}^n}} F(u, v, w) = -u^\top a - v^\top b + \varepsilon \sum_{i,j=1}^n \exp\left(\frac{u_i + v_j - c_{ij}(w)}{\varepsilon}\right) a_i b_j - \varepsilon, \quad (16)$$

where $\mathbb{R}_a^m = \{u \in \mathbb{R}^m : a^\top u = 0\}$.

We apply the block coordinate descent method to solve (16) with exact minimization for the two blocks u, v . For the block w , we use one step of the projected gradient descent method. This creates a hybrid combination of the classic BCD algorithm and the block coordinate gradient projection (BCGP) in [3]. The updating scheme of the hybrid block coordinate descent algorithm (HBCD) is given as follows:

$$\begin{aligned} u^{k+1} &= \arg \min_{u \in \mathbb{R}_a^m} \varphi_u^k(u) &= -\varepsilon \log \left(\exp\left(\frac{-C(w^k)}{\varepsilon}\right) (\exp(v^k/\varepsilon) \circ b) \right) + \lambda^k \mathbb{1}, \\ v^{k+1} &= \arg \min_{v \in \mathbb{R}^n} \varphi_v^k(v) &= -\varepsilon \log \left(\exp\left(\frac{-C(w^k)^\top}{\varepsilon}\right) (\exp(u^{k+1}/\varepsilon) \circ a) \right), \\ w^{k+1} &= \arg \min_{w \in [0,1]} \varphi_w^k(w) &= \text{Proj}_{[0,1]} \left(w^k - \eta \nabla_w F(u^{k+1}, v^{k+1}, w^k) \right), \end{aligned} \quad (17)$$

where the upper-bound functions associated with the blocks u, v, w are

$$\begin{aligned} \varphi_u^k(u) &= F(u, v^k, w^k), \\ \varphi_v^k(v) &= F(u^{k+1}, v, w^k), \\ \varphi_w^k(w) &= F(u^{k+1}, v^{k+1}, w^k) + \nabla_w F(u^{k+1}, v^{k+1}, w^k) (w - w^k) + \frac{1}{2\eta} (w - w^k)^2, \end{aligned} \quad (18)$$

with $\lambda^k = \varepsilon a^\top \log(\exp(\frac{-C(w^k)}{\varepsilon})(\exp(v^k/\varepsilon) \circ b))$ as the normalizing constant that enforces the extra constraint $a^\top u = 0$ and η is the stepsize.

If the stepsize satisfies $\eta \leq 1/L_w$, with L_w denoting the Lipschitz constant corresponding to the block w of $\nabla_w F$ [3, eq. (2.3)], then $\varphi_w^k(w)$ is a valid upper-bound function. In this case, the proposed HBCD algorithm belongs to the class of block successive upper-bound minimization (BSUM) methods [37, 25], which address minimization problems by iteratively minimizing block-wise surrogate upper bounds of the objective. Based on [7, 3, 37, 25], we derive convergence guarantees for HBCD.

Lemma 3.1 and lemma 3.3 below follow directly from the results in [7] and [3]. For completeness, we include their full proofs in the Appendix B, D.

Lemma 3.1 (boundedness of iterates). *For every $k \geq 1$, the iterates generated by (17) satisfy the bounds*

$$\|u^k\|_\infty \leq 2\|C\|_\infty, \quad \|v^k\|_\infty \leq 3\|C\|_\infty,$$

where $\|C\|_\infty = \max_{w \in [0,1]} \{\|C(w)\|_\infty\} = \max\{\|C(0)\|_\infty, \|C(1)\|_\infty\}$.

Lemma 3.2 (block Lipschitz continuity of $\nabla_w F$). *Let $\xi^k := (u^k, v^k, w^k)$ be the sequence generated by (17). For any $k \geq 1$ and $(w, w') \in [0,1]^2$, we have*

$$|\nabla_w F(u^k, v^k, w) - \nabla_w F(u^k, v^k, w')| \leq (\|\tilde{C}\|_\infty^2 / \varepsilon) \exp\left(\frac{6\|C\|_\infty}{\varepsilon}\right) |w - w'|, \quad (19)$$

where $\|\tilde{C}\|_\infty = \max\{\|x_i - y_j\|_p^p - |t_i - s_j|^p : i \in [m], j \in [n]\}$.

Proof. See Appendix C. □

Lemma 3.3 (sufficient descent property). *Let $\zeta^k := (u^k, v^k, w^k)$ and $\zeta^{k+1} := (u^{k+1}, v^{k+1}, w^{k+1})$ be generated by (17) with $\eta = (\varepsilon/\|\tilde{C}\|_\infty^2) \exp(\frac{-6\|C\|_\infty}{\varepsilon})$, then the following inequality holds:*

$$F(\zeta^k) - F(\zeta^{k+1}) \geq \kappa \left(\|u^k - u^{k+1}\|_{L^2(a)}^2 + \|v^k - v^{k+1}\|_{L^2(b)}^2 \right) + \tau |w^k - w^{k+1}|^2,$$

where $\kappa = \exp(\frac{-6\|C\|_\infty}{\varepsilon})/2\varepsilon$, $\tau = \|\tilde{C}\|_\infty^2 \exp(\frac{6\|C\|_\infty}{\varepsilon})/2\varepsilon$. In the above, $\|u^k - u^{k+1}\|_{L^2(a)}^2 = \sum_{i=1}^m (u_i^{k+1} - u_i^k)^2 a_i$, and $\|v^k - v^{k+1}\|_{L^2(b)}^2$ is similarly defined.

Relying on the preceding lemmas, we invoke [37] to establish the asymptotic convergence of the iterations (17) and employ the techniques of [25] to obtain the sublinear convergence rate.

Theorem 3.4. *Let $\tilde{\mathcal{S}}$ be the optimal solution set of (16) and $\{\xi^k\}$ be the sequence generated by the (17) with $\eta = (\varepsilon/\|\tilde{C}\|_\infty^2) \exp(\frac{-6\|C\|_\infty}{\varepsilon})$. Then ξ^k converges to $\tilde{\mathcal{S}}$ in the sense that*

$$\lim_{k \rightarrow \infty} \inf_{\xi \in \tilde{\mathcal{S}}} \|\xi^k - \xi\|_2 = 0.$$

Proof. To prove the convergence of HBCD, it is sufficient to show that HBCD iterates (17) and the objective function $F(\cdot)$ in (16) satisfy the assumption in [37, theorem 2-b].

First, Lemma 3.1 implies that the iterates generated by HBCD lie in a compact set.

Second, the upper-bound functions φ_u^k and φ_v^k in (18) satisfy [37, Assumption 2]. Moreover, by lemma 3.2 and the block descent lemma [3, Lemma 3.2], the function φ_w^k also satisfies this assumption.

Third, the strict convexity of the upper-bound functions guarantees that their corresponding minimization subproblems admit unique solutions. Moreover, the differentiability of $F(\xi)$ ensures the regularity condition. Hence, by [37, Theorem 2-b], the sequence $\{\xi^k\}$ generated by HBCD (17) converges to the set of stationary points, which in our case is the set of optimal solution due to the convexity of $F(\cdot)$. \square

Lemma 3.5. *Let $\tilde{\mathcal{S}}$ be the optimal solutions set of (16). There exists $\xi^* = (u^*, v^*, w^*) \in \tilde{\mathcal{S}}$ such that $\|u^*\|_\infty \leq 2\|C\|_\infty$ and $\|v^*\|_\infty \leq 3\|C\|_\infty$.*

Proof. See Appendix E. \square

Theorem 3.6. *Let $\zeta^k = (u^k, v^k, w^k)$ be the sequence generated by the iterations (17) with $\eta = (\varepsilon/\|\tilde{C}\|_\infty^2) \exp(\frac{-6\|C\|_\infty}{\varepsilon})$. For any $k \geq 1$, we have*

$$F(\zeta^k) - F^* \leq \frac{\rho_1 \rho_2}{k}, \quad (20)$$

where F^* denotes the optimal value of (16), $\rho_1 = (192m + 216n + 24) \frac{\|C\|_\infty^2}{\varepsilon} \exp(\frac{18\|C\|_\infty}{\varepsilon})$, $\rho_2 = \max\{4/\rho_1 - 2, F(\zeta^1) - F^*, 2\}$.

Proof. See Appendix F. \square

We conclude this section by reformulating HBCD into an efficient and easily implementable algorithm (Algorithm 1), with several remarks:

- To reduce computational cost, define $g = a \circ \exp(u/\varepsilon)$, $h = b \circ \exp(v/\varepsilon)$, $K(w) = \exp(-C(w)/\varepsilon)$. Then the HBCD iteration can be simplified to a Sinkhorn-like algorithm.

- Algorithm 1 provides a competitive framework for solving the eTiOT problem. By skipping the normalization step (17), and updating w and the stopping criterion only once every `freq` iterations, it avoids redundant operations and reduces computation without compromising the convergence.

Algorithm 1 HBCD algorithm for solving eTiOT problem (7).

```

1: Input two discrete distributions  $\alpha = \sum_{i=1}^m a_i \delta_{(x_i, t_i)}$  and  $\beta = \sum_{j=1}^n b_j \delta_{(y_j, s_j)}$ , entropic regularization parameter  $\varepsilon > 0$ ,  $\eta$ , freq.
2: Initialize  $\Gamma \in \mathbb{R}^{m \times n}$  defined by  $\Gamma_{ij} = \|x_i - y_j\|_2^2$ ,
3:  $\Phi \in \mathbb{R}^{m \times n}$  defined by  $\Phi_{ij} = |t_i - s_j|^2$ ,
4:  $w = 0.5$ ,  $C = w\Gamma + (1-w)\Phi$ ,  $K = \exp(-C/\varepsilon)$ ,  $h = \frac{1}{m}\mathbb{1}_m$ ,
5: while termination criteria not met do
6:    $g \leftarrow a \oslash (Kh)$ 
7:    $h \leftarrow b \oslash (K^\top g)$ 
8:   if  $\text{mod}(t, \text{freq}) = 0$  then
9:      $w \leftarrow \max \{ \min \{ w - \eta [g^\top ((\Phi - \Gamma) \circ K)h], 1 \}, 0 \}$ 
10:     $C \leftarrow w\Gamma + (1-w)\Phi$ 
11:     $K \leftarrow \exp(-C/\varepsilon)$ 
12:   end if
13: end while
14:  $\pi \leftarrow \text{Diag}(g) \cdot K \cdot \text{Diag}(h)$ ,  $\mathcal{D}_p^\varepsilon(\alpha, \beta) \leftarrow \langle C, \pi \rangle$ 
15: return  $\pi, w, \mathcal{D}_p^\varepsilon(\alpha, \beta)$ 

```

4 Experiments

In this section, we evaluate the empirical effectiveness of the proposed Time-integrated Optimal Transport (TiOT) problem through extensive numerical experiments. Specifically, we analyze the stability and reliability of the optimal solutions of the TiOT problem in Section 4.1; examine the properties of the induced distance in Section 4.2, validate the theoretical convergence and demonstrate the algorithmic benefits of the entropic variant (eTiOT) in Section 4.3; and finally, we apply TiOT to time series classification problem on several standard datasets in Section 4.4. All experiments are implemented in Python and executed on a machine equipped with a 12th Gen Intel(R) Core(TM) i7-1260P 2.10 GHz processor. The source code is available at <https://github.com/Thai-npd/TiOT-code>

For all experiments in this section, we consider distributions $\alpha = \sum_{i=1}^m a_i \delta_{(x_i, t_i)}$ and $\beta = \sum_{j=1}^n b_j \delta_{(y_j, s_j)}$ with uniform weights, $a = \frac{1}{m}\mathbb{1}_m$ and $b = \frac{1}{n}\mathbb{1}_n$, where $\{x_i\}$ and $\{t_i\}$ are standardized using Z-score normalization; Similarly for $\{y_j\}$ and $\{s_j\}$.

In Sections 4.3, 4.4, the eTiOT problem is solved by Algorithm 1 with termination criterion $\|g \circ (Kh) - a\|_1 < 0.005$, adopted from [46] for fair comparisons. To improve efficiency, multiple subiterations are performed for the w -block in each iteration: Projected Gradient Descent is repeated until successive changes in w fall below 10^{-7} for small-scale problems ($n, m < 1000$) or 10^{-2} for large-scale ones, with at most 50 subiterations. The stepsize is set as $\eta = \sigma/20$ if $\sigma \geq 10$ and $\eta = \sigma/10$ otherwise, where $\sigma = \frac{1}{\varepsilon}(g^\top ((\Phi - \Gamma)^2 \circ K)h)$ approximates the local curvature constant in w of the objective minimized by Algorithm 1.

4.1 Robustness of TiOT

In this section, we illustrate the robustness of the transportation plan π generated by our proposed model TiOT compared to the transportation plan induced by the usual Wasserstein distance with the base metric $d_{2,w}$, that is, $\mathcal{W}_{2,w}$.

Dataset and experiment design In this experiment, we generate two mixture of Gaussians time series $\alpha = \sum_{i=1}^m a_i \delta_{(x_i, t_i)}$ and $\beta = \sum_{j=1}^n b_j \delta_{(y_j, s_j)}$ by letting $m = n = 200$, $a_i = b_i = 1/200$, and $t_i = s_i = i$ for any $i = 1, \dots, 200$. In addition, we generate x_i and y_j by

$$\begin{aligned} x_i &= 0.2 \exp\left(-\frac{(t_i-50)^2}{2 \times 7^2}\right) + \exp\left(-\frac{(t_i-140)^2}{2 \times 10^2}\right) + \mathcal{N}(0, 0.01^2), \\ y_i &= 0.2 \exp\left(-\frac{(t_i-75)^2}{2 \times 7^2}\right) + \exp\left(-\frac{(t_i-165)^2}{2 \times 10^2}\right) + \mathcal{N}(0, 0.01^2), \end{aligned} \quad (21)$$

for any $i = 1, \dots, 200$ and $\mathcal{N}(0, 0.01^2)$ is Gaussian noise. In Figure 1, we visualize these two mixtures of Gaussians in blue and red, respectively. Finally, we compute $\mathcal{W}_{2,w}$ with $w = 0.1$ and 0.8 to obtain the transportation plan π , and solve our proposed TiOT problem to get both optimal parameter w^* and transportation plan π^* . In Figure 1, each green line represents a non-zero entry $\pi_{i,j}$.

Analysis We first note that all three alignments are indeed one-to-one alignments, a finding consistent with the fact that one of optimal plans between two discrete distributions of the same size and uniform weight must be a permutation [35]. However, the resulting alignment changes significantly when w changes. For instance, the temporal constraint imposed by $\mathcal{W}_{2,w=0.1}$ proves overly rigid, preventing the correct alignment of the two peaks. Conversely, $\mathcal{W}_{2,w=0.8}$ is too permissive, leading to multiple mismatches. In contrast, TiOT adaptively selects w to maximize $\mathcal{W}_{2,w}$, thereby discouraging pairings that might otherwise appear optimal under a poorly chosen weight. This allows TiOT to avoid overfitting and yield a more robust and balanced alignment.

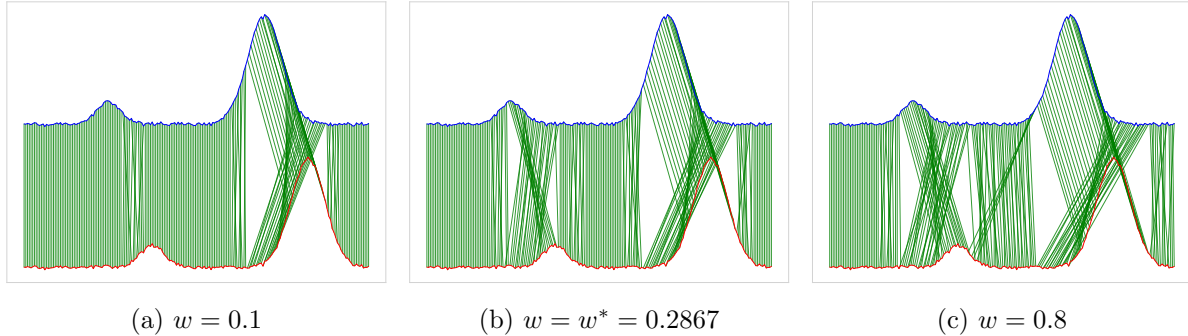


Figure 1: Alignment (transportation) map π between two time series. Left and right: π induced by $\mathcal{W}_{2,w}$ with selected $w = 0.1$ and $w = 0.8$, middle: π^* induced by our proposed TiOT model.

4.2 Time Series Analysis with \mathcal{D}_2 and $\mathcal{W}_{2,w}$ metrics

In this section, we compare the proposed metric \mathcal{D}_2 with $\mathcal{W}_{2,w}$ on a time series lag analysis task. While the performance of $\mathcal{W}_{2,w}$ is highly sensitive to its parameter w , \mathcal{D}_2 avoids this limitation through its auto-selection mechanism, yielding a more robust and reliable metric.

Dataset and experiment design The dataset contains daily temperature of Delhi, India, from January 1, 2013, to January 1, 2017 [41], denoted by $x = (x_1, \dots, x_{1462}) \in \mathbb{R}^{1462}$. A one-year time series starting on day ℓ is defined as

$$x^{(\ell)} := (x_\ell, x_{\ell+1}, \dots, x_{\ell+364}) \in \mathbb{R}^{365},$$

for $\ell = 1, 2, \dots, 730$. We then measure the dissimilarity between the initial series $x^{(1)}$ and its lagged versions $x^{(\ell)}$ using \mathcal{D}_2 (2.7) and $\mathcal{W}_{2,w}$ with fixed parameters $w = 0.2, 0.5, 0.8$.

Analysis In Figure 2 (left subplot), we report the values of \mathcal{D}_2 and $\mathcal{W}_{2,w}$ between $x^{(1)}$ and $x^{(\ell)}$ against ℓ , where $\ell = 1, 2, \dots, 730$. All metrics capture the annual periodicity of the climate data, with dissimilarity values minimized near lags of 365 and 730, correctly reflecting seasonal similarity. However, for off-cycle lags such as when $\ell \in [100, 300]$ or $\ell \in [450, 650]$, the values of the metrics varies significantly. With a low weight on the temperature values ($w = 0.2$), the $\mathcal{W}_{2,0.2}$ produces an almost perfect sinusoid. Since the cost is defined as $d_{2,w}^2 = w\|x - y\|_2^2 + (1 - w)(t - s)^2$, thus $\mathcal{W}_{2,0.2}$ recognizes the temporal shift but ignores the influence of the temperature variations. On the other hand, a higher weight ($w = 0.8$) returns a counter-intuitive result: $\mathcal{W}_{2,0.8}(x^{(180)}, x^{(0)}) < \mathcal{W}_{2,0.8}(x^{(90)}, x^{(0)})$. This contradicts the natural expectation that a six-month shift should exceed a three-month one; similar behavior occurs for $w = 0.5$ and in the second year. In short, low w ignores temperature information, while high w distorts temporal relationships. In contrast, our proposed \mathcal{D}_2 , interpretable as a maximum over all $\mathcal{W}_{2,w}$, achieves a robust balance between time and temperature, hence, retains temperature-specific fluctuations while clearly reflecting the seasonal cycle.

In Figure 2 (right subplot), we analyze the sensitivity of $\mathcal{W}_{2,w}$ with respect to its weight parameter. We plot $\mathcal{W}_{2,w}$ against $w \in [0, 1]$ for fixed shifts $\ell \in \{30, 90, 180, 270\}$ (days). When ℓ is small (e.g., $\ell = 30$), the $\mathcal{W}_{2,w}$ metric is relatively insensitive to w , consistently yielding low dissimilarity values. For larger shifts ($\ell = 90, 180, 270$), however, the choice of w becomes critical: $\mathcal{W}_{2,w}$ varies substantially, and different values of w even change the ordering of which shift appears more significant. For example, when $w \in [0.15, 0.35]$, $\mathcal{W}_{2,w}$ considers $\ell = 180$ to be more significant, while for $w \in [0.4, 0.6]$, it considers $\ell = 90$ to be more significant. By contrast, our TiOT framework resolves this ambiguity by selecting the maximizer w for each pair of series, thereby providing a robust, parameter-free, and worst-case measure that is both consistent and reliable.

4.3 Numerical performance of entropic TiOT

In this section, we provide numerical experiments to validate our theoretical and computational findings.

First, we demonstrate our theoretical result in Theorem 2.9, that is, the convergence of the entropic TiOT (eTiOT) to the exact TiOT as the regularization parameter ϵ approaches zero. For this experiment, we set $n = m = 100$ and generate two mixtures of Gaussians time series, similar to the procedure in Section 4.1. We then solve the exact TiOT via its linear programming (LP) formulation (Appendix G) and its entropic regularized counterpart, eTiOT (7) via Algorithm 1 for a range of regularization parameters $\epsilon = 1/2, 1/10, 1/50, 1/100$. This process was repeated 100 times with different random seeds. Figure 3 (left subplot) reports the distribution of deviations between the optimal objective values and the corresponding solutions of the two problems. One can observe that both differences decrease to 0 as $\epsilon \rightarrow 0$. This result

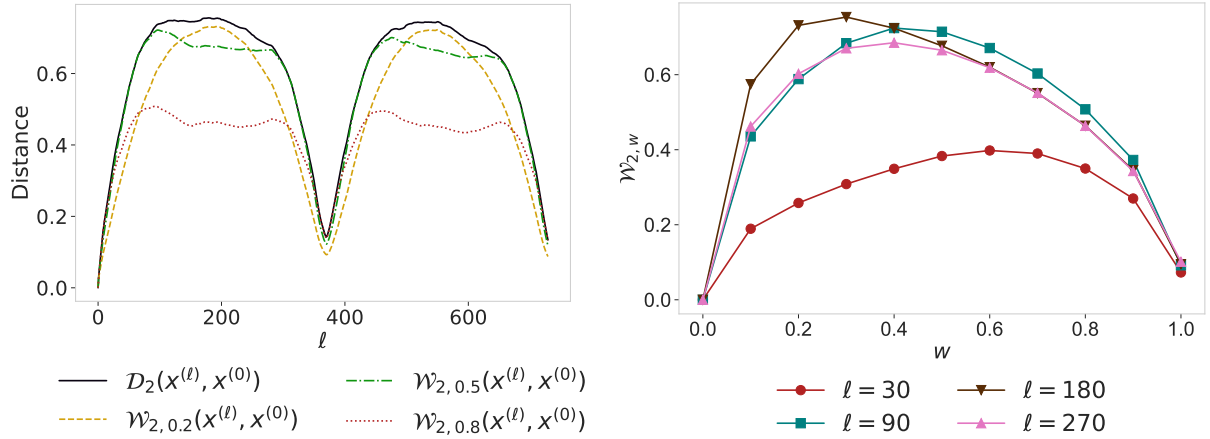


Figure 2: Left: \mathcal{D}_2 and $\mathcal{W}_{2,w}$ between $x^{(0)}$ and $x^{(\ell)}$. Right: $\mathcal{W}_{2,w}$ metric against w .

empirically verifies our theoretical analysis, showing that eTiOT serves as a reliable and accurate approximation of TiOT.

Second, we evaluate the computational complexity of our proposed algorithm against several relevant benchmarks. Specifically, we compare running time of solving the eTiOT problem (7) via Algorithm 1 against its LP counterpart TiOT (37), as well as the standard OT (3) and its entropic regularized version eOT, with the base metric $d_{2,w}$ and fixed parameter $w = 0.5$. For both eTiOT and eOT, we set the regularization parameter $\varepsilon = 0.1$ and the tolerance = 0.005. Figure 3 (right subplot) reports the running time required to solve each problem as the length of the time series $n = m$ increases. As expected, the performance of TiOT, formulated as a large-scale LP, quickly becomes computationally prohibitive. The standard OT, solved by a standard Python Optimal Transport library ([17, 18]), also exhibits poor scaling. In contrast, Algorithm 1 shows a significant performance advantage, requiring only about 2–3 times the runtime of the highly efficient Sinkhorn algorithm for the classical eOT.

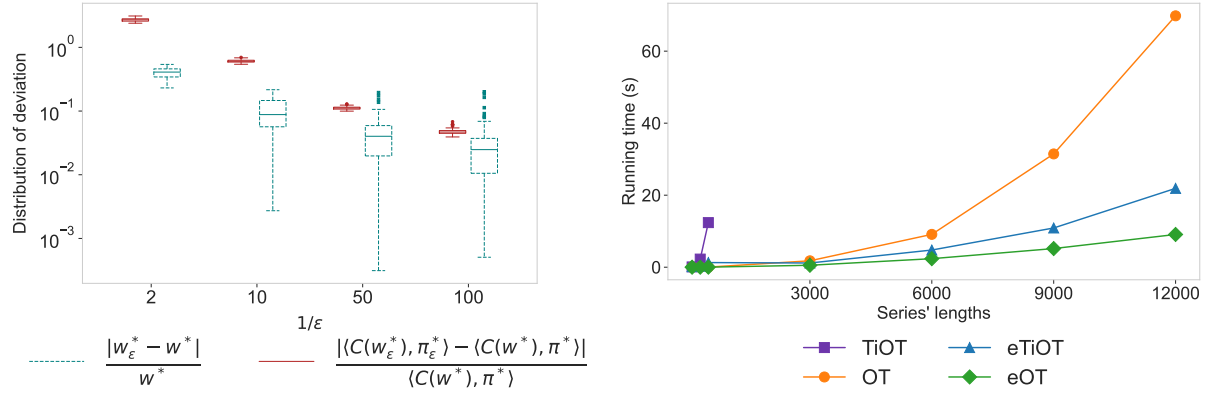


Figure 3: Left: Deviation of TiOT and eTiOT. Right: Computational comparison.

4.4 Experiments on 1NN classification

In this section, we assess the effectiveness of the distance defined by the TiOT problem for time series classification tasks. In particular, we compare the classification errors of the 1-nearest-neighbor algorithm using the following base metrics: Euclidean (ED), Dynamic Time Warping (DTW) with learned warping window [11], eTiOT (Algorithm 1), and eTAOT (Algorithm 1 in [46])¹ on 15 datasets obtained from the UCR time series archive [12]. For ED and DTW, we adopt the classification errors provided by the benchmark website [12].

First, the overall classification errors of ED, DTW, eTiOT, and eTAOT(ω) are presented in Table 1. Both DTW and eTAOT(ω) require a parameter controlling the strength of temporal constraints; these parameters are selected via leave-one-out cross-validation (LOOCV) in [11, 46], yielding learned_w for DTW and w_{grid} for eTAOT. For the regularization parameter ε of eTiOT and eTAOT(ω), we perform 3-fold cross-validation over the grid $\{0.01, 0.02, \dots, 0.1\}$.

Second, we verify the robustness of the eTiOT metric compared with eTAOT(ω) for fixed w by plotting classification errors across the range $\varepsilon \in \{0.01, 0.02, \dots, 0.1\}$. For eTAOT(ω), we use the previously tuned w_{grid} from LOOCV [46]; additionally, we include $\omega = w_{\text{grid}}/5$ and $\omega = 5w_{\text{grid}}$ to provide a more comprehensive comparison. Performance on 3 of the 15 datasets is shown in Figure 4, while results for the remaining datasets are presented in Figure 5 (Appendix H).

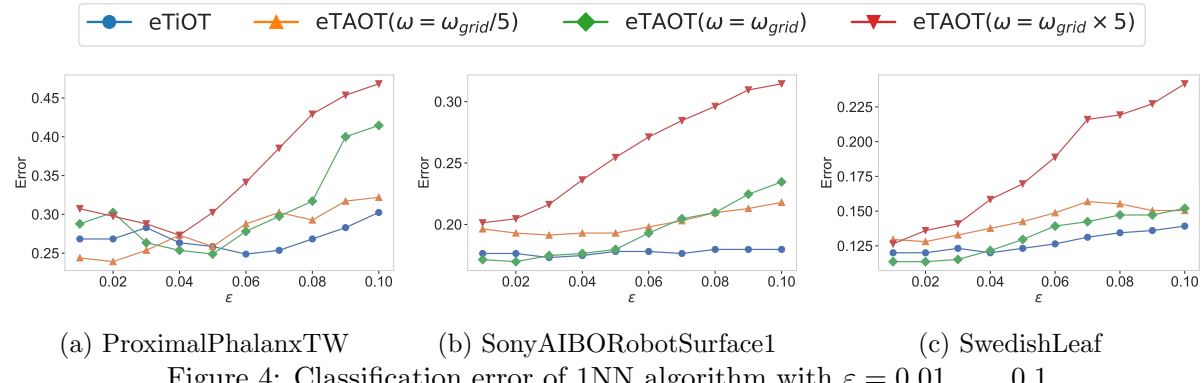


Figure 4: Classification error of 1NN algorithm with $\varepsilon = 0.01, \dots, 0.1$.

From Table 1, the 1NN algorithm using the eTiOT metric achieves the lowest error on 10 of the 15 datasets. Specifically, its performance is better than or equal to ED on 12/15 datasets, DTW on 12/15 datasets, and eTAOT on 11/15 datasets. These results demonstrate both the effectiveness and the stability of eTiOT, highlighting its reliability as a dissimilarity measure for time series. Notably, eTiOT is the only metric in this experiment that does not require cross-validation to tune the strength of temporal constraints, relying instead on an adaptive mechanism. The robustness of eTiOT is further illustrated in Figure 4, where the line representing eTiOT errors generally exhibits a slower increase as ε grows from 0.01 to 0.1. It is well known that a larger regularization parameter typically reduces the running time of the entropic-regularized optimal transport problem. Therefore, this behavior not only provides additional evidence of eTiOT's robustness but also justifies the use of larger ε values for faster computations.

¹eTAOT $_{\omega}(\alpha, \beta) = \langle C(\omega), \pi_{\varepsilon}^* \rangle$ where $\pi_{\varepsilon}^* = \arg \min_{\pi \in \Pi(\alpha, \beta)} \langle C(w), \pi \rangle + \mathbf{KL}(\pi | a \circ b)$ and $c_{ij}(\omega) = \|x - y\|_2^2 + \omega(t_i - s_j)^2$

Table 1: Comparison of classification errors for eTiOT, Euclidean, DTW, and eTAOT.

dataset	train/test size	length	error rates			
			ED	DTW	eTAOT	eTiOT
Adiac	390/391	176	0.389	0.391	0.327	0.297
ArrowHead	36/175	251	0.200	0.200	0.263	0.251
BirdChicken	20/20	512	0.450	0.300	0.300	0.200
CBF	30/900	128	0.148	0.004	0.011	0.004
DistalPhalanxOAG	400/139	80	0.374	0.374	0.324	0.317
DistalPhalanxOC	600/276	80	0.283	0.275	0.261	0.257
DistalPhalanxTW	600/276	80	0.367	0.367	0.367	0.353
Ham	109/105	431	0.400	0.400	0.390	0.362
MiddlePhalanxOAG	400/154	80	0.481	0.481	0.487	0.468
MiddlePhalanxOC	600/291	80	0.234	0.234	0.258	0.268
MiddlePhalanxTW	600/291	80	0.487	0.494	0.455	0.422
ProximalPhalanxOC	400/205	80	0.192	0.209	0.199	0.206
ProximalPhalanxTW	400/205	80	0.293	0.244	0.249	0.268
SonyAIBORobotSurface1	20/601	70	0.305	0.305	0.234	0.180
SwedishLeaf	500/625	128	0.211	0.154	0.114	0.120

5 Conclusions

In this work, we introduce *Time-integrated Optimal Transport* (TiOT), a new framework for comparing time series. TiOT automatically balances temporal and feature information, thereby eliminating the need for manual parameter tuning compared to other measures. Moreover, we show that TiOT defines a proper metric that preserves fundamental properties of Wasserstein spaces.

We further develop an entropic regularized variant, eTiOT, and prove that it serves as a reliable approximation of TiOT. To solve eTiOT efficiently, we propose a Block Coordinate Descent (BCD) algorithm and provide a rigorous convergence analysis. Extensive experiments on synthetic and real-world datasets demonstrate the practical effectiveness and computational efficiency of our approach. Finally, TiOT offers a generalizable theoretical and practical foundation for defining a robust, adaptively tuned, weighted Euclidean distance between arbitrary data vectors.

References

- [1] Martin Arjovsky, Soumith Chintala, and Léon Bottou. Wasserstein generative adversarial networks. In *Proceedings of the 34th International Conference on Machine Learning*, volume 70 of *Proceedings of Machine Learning Research*, pages 214–223. PMLR, 06–11 Aug 2017.
- [2] Daniel Bartl, Mathias Beiglböck, and Gudmund Pammer. The Wasserstein space of stochastic processes. *Journal of the European Mathematical Society*, 12 2024.
- [3] Amir Beck and Luba Tetruashvili. On the convergence of block coordinate descent type methods. *SIAM Journal on Optimization*, 23(4):2037–2060, 2013.
- [4] Jean-David Benamou, Guillaume Carlier, Marco Cuturi, Luca Nenna, and Gabriel Peyré. Iterative Bregman projections for regularized transportation problems. *SIAM Journal on Scientific Computing*, 37(2):A1111–A1138, 2015.

- [5] Nicolas Bonneel, Gabriel Peyré, and Marco Cuturi. Wasserstein barycentric coordinates: histogram regression using optimal transport. *ACM Trans. Graph.*, 35(4), July 2016.
- [6] Yann Brenier. The least action principle and the related concept of generalized flows for incompressible perfect fluids. *Journal of the American Mathematical Society*, 2(2):225–255, 1989.
- [7] Guillaume Carlier. On the linear convergence of the multimarginal Sinkhorn algorithm. *SIAM Journal on Optimization*, 32(2):786–794, 2022.
- [8] Angus A. Cook, Göksel Mısrılı, and Zhong Fan. Anomaly detection for iot time series data: A survey. *IEEE Internet of Things Journal*, 7(7):6481–6494, 2020.
- [9] Nicolas Courty, Rémi Flamary, Devis Tuia, and Alain Rakotomamonjy. Optimal transport for domain adaptation. *IEEE Transactions on Pattern Analysis and Machine Intelligence*, 39(9):1853–1865, 2017.
- [10] Marco Cuturi. Sinkhorn distances: Lightspeed computation of optimal transport. In *Advances in Neural Information Processing Systems*, volume 26. Curran Associates, Inc., 2013.
- [11] Hoang Anh Dau, Anthony Bagnall, Kaveh Kamgar, Chin-Chia Michael Yeh, Yan Zhu, Shaghayegh Gharghabi, Chotirat Ann Ratanamahatana, and Eamonn Keogh. The ucr time series archive. *IEEE/CAA Journal of Automatica Sinica*, 6(6):1293–1305, 2019.
- [12] Hoang Anh Dau, Eamonn Keogh, Kaveh Kamgar, Chin-Chia Michael Yeh, Yan Zhu, Shaghayegh Gharghabi, Chotirat Ann Ratanamahatana, Yanping, Bing Hu, Nurjahan Begum, Anthony Bagnall, Abdullah Mueen, Gustavo Batista, and Hexagon-ML. The ucr time series classification archive, October 2018. https://www.cs.ucr.edu/~eamonn/time_series_data_2018/.
- [13] Luca De Gennaro Aquino and Stephan Eckstein. Minmax methods for optimal transport and beyond: Regularization, approximation and numerics. In *Advances in Neural Information Processing Systems*, volume 33, pages 13818–13830. Curran Associates, Inc., 2020.
- [14] Sofien Dhouib, Ievgen Redko, Tanguy Kerdoncuff, Rémi Emonet, and Marc Sebban. A swiss army knife for minimax optimal transport. In *Proceedings of the 37th International Conference on Machine Learning*, volume 119 of *Proceedings of Machine Learning Research*, pages 2504–2513. PMLR, 13–18 Jul 2020.
- [15] Stephan Eckstein and Gudmund Pammer. Computational methods for adapted optimal transport. *The Annals of Applied Probability*, 34(1A):675 – 713, 2024.
- [16] Ivar Ekeland. An optimal matching problem. *ESAIM: Control, Optimisation and Calculus of Variations*, 11(1):57–71, 2005.
- [17] Rémi Flamary, Nicolas Courty, Alexandre Gramfort, Mokhtar Z. Alaya, Aurélie Boisbunon, Stanislas Chambon, Laetitia Chapel, Adrien Corenflos, Kilian Fatras, Nemo Fournier, Léo Gautheron, Nathalie T.H. Gayraud, Hicham Janati, Alain Rakotomamonjy, Ievgen Redko, Antoine Rolet, Antony Schutz, Vivien Seguy, Danica J. Sutherland, Romain Tavenard, Alexander Tong, and Titouan Vayer. Pot: Python optimal transport. *Journal of Machine Learning Research*, 22(78):1–8, 2021.

[18] Rémi Flamary, Cédric Vincent-Cuaz, Nicolas Courty, Alexandre Gramfort, Oleksii Kachaiev, Huy Quang Tran, Laurène David, Clément Bonet, Nathan Cassereau, Théo Gnassounou, Eloi Tanguy, Julie Delon, Antoine Collas, Sonia Mazelet, Laetitia Chapel, Tanguy Kerdoncuff, Xizheng Yu, Matthew Feickert, Paul Krzakala, Tianlin Liu, and Eduardo Fernandes Montesuma. *Pot python optimal transport* (version 0.9.5), 2024.

[19] Joel Franklin and Jens Lorenz. On the scaling of multidimensional matrices. *Linear Algebra and its Applications*, 114-115:717–735, 1989. Special Issue Dedicated to Alan J. Hoffman.

[20] Uriel Frisch, Sabino Matarrese, Roya Mohayaee, and Andrei Sobolevski. A reconstruction of the initial conditions of the universe by optimal mass transportation. *Nature*, 417(6886):260–262, 2002.

[21] Charlie Frogner, Chiyuan Zhang, Hossein Mobahi, Mauricio Araya, and Tomaso A. Poggio. Learning with a Wasserstein loss. In *Advances in Neural Information Processing Systems (NeurIPS)*, pages 2053–2061, 2015.

[22] Wilfrid Gangbo and Robert J. McCann. Shape recognition via Wasserstein distance. *Quarterly of Applied Mathematics*, 58(4):705–737, 2000.

[23] Clive William John Granger and Paul Newbold. *Forecasting economic time series*. Academic press, 2014.

[24] Steven Haker, Lei Zhu, Allen Tannenbaum, and Sigurd Angenent. Optimal mass transport for registration and warping. *International Journal of Computer Vision*, 60(3):225–240, 2004.

[25] Mingyi Hong, Xiaoyun Wang, Meisam Razaviyayn, and Zhi-Quan Luo. Iteration complexity analysis of block coordinate descent methods. *Mathematical Programming*, 163(1):85–114, 2017.

[26] Minhui Huang, Shiqian Ma, and Lifeng Lai. On the convergence of projected alternating maximization for equitable and optimal transport. *Journal of Machine Learning Research*, 25(1), January 2024.

[27] Brijnesh Jain. Revisiting inaccuracies of time series averaging under dynamic time warping. *Pattern Recognition Letters*, 125:418–424, 2019.

[28] Pratik Jawanpuria, N.T.V. Satyadev, and Bamdev Mishra. Efficient robust optimal transport with application to multi-label classification. In *2021 60th IEEE Conference on Decision and Control (CDC)*, page 1490–1495. IEEE Press, 2021.

[29] Richard Jordan, David Kinderlehrer, and Felix Otto. The variational formulation of the Fokker–Planck equation. *SIAM Journal on Mathematical Analysis*, 29(1):1–17, 1998.

[30] Leonid Vitalievich Kantorovich. On the translocation of masses. *Dokl. Akad. Nauk SSSR*, 37:199–201, 1942.

[31] L. Mico, J. Oncina, and E. Vidal. An algorithm for finding nearest neighbours in constant average time with a linear space complexity. In *Proceedings., 11th IAPR International Conference on Pattern Recognition. Vol.II. Conference B: Pattern Recognition Methodology and Systems*, pages 557–560, 1992.

[32] Gaspard Monge. Mémoire sur la théorie des déblais et des remblais. *Histoire de l'Académie Royale des Sciences de Paris*, 1781.

[33] Mohammad Amin Morid, Olivia R Liu Sheng, and Joseph Dunbar. Time series prediction using deep learning methods in healthcare. *ACM Transactions on Management Information Systems*, 14(1):1–29, 2023.

[34] François-Pierre Paty and Marco Cuturi. Subspace robust Wasserstein distances. In *Proceedings of the 36th International Conference on Machine Learning*, volume 97 of *Proceedings of Machine Learning Research*, pages 5072–5081. PMLR, 09–15 Jun 2019.

[35] Gabriel Peyre and Marco Cuturi. Computational optimal transport. *Foundations and Trends in Machine Learning*, 11(5-6):355–607, 2019.

[36] M. S. Pinsker. *Information and Information Stability of Random Variables and Processes*. Holden-Day, Inc., San Francisco, Calif.-London-Amsterdam, 1964.

[37] Meisam Razaviyayn, Mingyi Hong, and Zhi-Quan Luo. A unified convergence analysis of block successive minimization methods for nonsmooth optimization. *SIAM Journal on Optimization*, 23(2):1126–1153, 2013.

[38] H. Sakoe and S. Chiba. Dynamic programming algorithm optimization for spoken word recognition. *IEEE Transactions on Acoustics, Speech, and Signal Processing*, 26(1):43–49, 1978.

[39] Filippo Santambrogio. *Optimal Transport for Applied Mathematicians*. Progress in Nonlinear Differential Equations and Their Applications. Birkhäuser, Cham, 2015.

[40] Kaiwen Shi. Time parameterized optimal transport. *arXiv preprint*, arXiv:2502.10607, 2025.

[41] Sumanthvrao. Daily climate time series data. <https://www.kaggle.com/datasets/sumanthvrao/daily-climate-time-series-data?select=DailyDelhiClimateTrain.csv>. Accessed: 2025-09-28.

[42] Matthew Thorpe, Serim Park, Soheil Kolouri, Gustavo K. Rohde, and Dejan Slepčev. A transportation l^p distance for signal analysis. *Journal of Mathematical Imaging and Vision*, 59(2):187–210, October 2017.

[43] Ruey S. Tsay. *Multivariate Time Series Analysis: With R and Financial Applications*. Wiley Series in Probability and Statistics. Wiley, 2014.

[44] Cédric Villani. *Topics in Optimal Transportation*. Graduate Studies in Mathematics. American Mathematical Society, 2003.

[45] Cédric Villani. *Optimal Transport*. Grundlehren der mathematischen Wissenschaften. Springer, 2009.

[46] Zheng Zhang, Ping Tang, and Thomas Corpetti. Time adaptive optimal transport: A framework of time series similarity measure. *IEEE Access*, 8:149764–149774, 2020.

A Proof of the existence of optimal solution of (3)

$$\mathcal{D}_p(\alpha, \beta) = \max_{w \in [0, 1]} \left[\min_{\pi \in \Pi(\alpha, \beta)} \int_{\mathbb{R}^{d+1} \times \mathbb{R}^{d+1}} d_{p,w}((x, t), (y, s))^p d\pi((x, t), (y, s)) \right]^{1/p}$$

By [39, Theorem 1.7], the inner minimization admits an optimal solution. To prove the existence of an optimal w^* , we invoke the Weierstrass theorem. Since $[0, 1]$ is compact, it remains to show that $\mathcal{T}_p(w) = \min_{\pi \in \Pi(\alpha, \beta)} \int d_{p,w}^p d\pi$ is upper semi-continuous with respect to $w \in [0, 1]$.

To this end, we show the openness of the preimage $\mathcal{T}_p^{-1}((-\infty, a)) = \{w \in [0, 1] : \mathcal{T}_p(w) < a\}$. Assume that $\mathcal{T}_p^{-1}((-\infty, a)) \neq \emptyset$, take an arbitrary $\bar{w} \in \mathcal{T}_p^{-1}((-\infty, a))$. Thus, there exists $\bar{\pi}$ such that $\int d_{p,\bar{w}}^p d\bar{\pi} < a$. Denote $J_{\bar{\pi}} : [0, 1] \rightarrow \mathbb{R}$ by $J_{\bar{\pi}}(w) = \int d_{p,w}^p d\bar{\pi}$. Since $J_{\bar{\pi}}(w)$ is continuous with respect to w , the set $J_{\bar{\pi}}^{-1}((-\infty, a)) = \{w \in [0, 1] : J_{\bar{\pi}}(w) < a\}$ is open. It follows that there exists $r > 0$ such that the ball $B(\bar{w}, r) \subset J_{\bar{\pi}}^{-1}((-\infty, a))$. Therefore, for all $w \in B(\bar{w}, r)$, we have $\mathcal{T}_p(w) \leq J_{\bar{\pi}}(w) < a$, which implies $B(\bar{w}, r) \subset \mathcal{T}_p^{-1}((-\infty, a))$. Hence $\mathcal{T}_p^{-1}((-\infty, a))$ is open, and consequently, $\mathcal{T}_p(w)$ is upper semi-continuous.

B Proof of lemma 3.1

First, we have the bounds $C_{j\ell}(w^{k-1}) \geq C_{i\ell}(w^{k-1}) - 2\|C(w^{k-1})\|_{\infty}$ for all $i, j = 1, \dots, m$, $k = 1, \dots, n$, which gives

$$\begin{aligned} u_i^k - u_j^k &= -\varepsilon \log \langle e^{\frac{-C_{i\cdot}(w^{k-1})}{\varepsilon}}, e^{\frac{v^{k-1}}{\varepsilon}} \circ b \rangle + \varepsilon \log \langle e^{\frac{-C_{j\cdot}(w^{k-1})}{\varepsilon}}, e^{\frac{v^{k-1}}{\varepsilon}} \circ b \rangle \\ &\leq -\varepsilon \log \langle e^{\frac{-C_{i\cdot}(w^{k-1})}{\varepsilon}}, e^{\frac{v^{k-1}}{\varepsilon}} \circ b \rangle + \varepsilon \log \langle e^{\frac{-C_{i\cdot}(w^{k-1})}{\varepsilon} + \frac{2\|C(w^{k-1})\|_{\infty}}{\varepsilon}}, e^{\frac{v^{k-1}}{\varepsilon}} \circ b \rangle \\ &= 2\|C(w^{k-1})\|_{\infty} \end{aligned}$$

where $C_{i\cdot}(w^{k-1})$ denotes the i -th row of $C(w^{k-1})$. Combining this inequality and the normalization property, for any $j = 1, \dots, m$, we have that $-u_j^k = \sum_{i=1}^m (u_i^k - u_j^k) a_i \leq 2\|C(w^{k-1})\|_{\infty}$ which implies

$$u_j^k \geq -2\|C(w^{k-1})\|_{\infty}.$$

Similarly, since $u_i^k = \sum_{j=1}^m (u_i^k - u_j^k) a_j \leq 2\|C(w^{k-1})\|_{\infty}$ for any $i = 1, \dots, m$, we have

$$u_i^k \leq 2\|C(w^{k-1})\|_{\infty}.$$

Combining above two inequalities, we have $\|u^k\|_{\infty} \leq 2\|C(w^{k-1})\|_{\infty} \leq 2\|C\|_{\infty}$. Now as $e^{\frac{-\|C(w^{k-1})\|_{\infty}}{\varepsilon}} \leq e^{\frac{-C_{\ell i}(w^{k-1})}{\varepsilon}}$ for any $\ell \in [m]$ and $i \in [n]$, we have for all $i \in [n]$,

$$v_i^k = -\varepsilon \log \sum_{\ell=1}^m e^{\frac{-C_{\ell i}(w^{k-1})}{\varepsilon}} e^{\frac{v_{\ell}^k}{\varepsilon}} a_{\ell} \leq -\varepsilon \log(e^{\frac{-\|C(w^{k-1})\|_{\infty} - 2\|C(w^{k-1})\|_{\infty}}{\varepsilon}}) = 3\|C(w^{k-1})\|_{\infty}.$$

Applying an analogous argument and using the bounds $e^{\frac{-C_{\ell i}(w^{k-1})}{\varepsilon}} \leq e^{\frac{\|C(w^{k-1})\|_{\infty}}{\varepsilon}}$, we have

$$v_i^k \geq -3\|C(w^{k-1})\|_{\infty} \quad \forall i \in [n].$$

Therefore, we get $\|v_i^k\|_{\infty} \leq 3\|C(w^{k-1})\|_{\infty} \leq 3\|C\|_{\infty}$.

C Proof of lemma 3.2

In the later part of this section, we shall frequently use the smoothness property of the exponential function over a bounded region; that is, given $M > 0$, for any $(a, b) \in [-M, M] \times [-M, M]$, we have

$$|e^b - e^a| \leq e^M |b - a|. \quad (22)$$

From this, we obtain

$$\begin{aligned} \text{LHS of (19)} &= \left| \sum_{i=1}^m \sum_{j=1}^n -\tilde{C}_{ij} \exp\left(\frac{u_i^k + v_j^k}{\varepsilon}\right) \left(\exp\left(\frac{-C_{ij}(w)}{\varepsilon}\right) - \exp\left(\frac{-C_{ij}(w')}{\varepsilon}\right) \right) a_i b_j \right| \\ &\leq (\|\tilde{C}\|_\infty^2 / \varepsilon) \sum_{i=1}^m \sum_{j=1}^n \exp\left(\frac{u_i^k + v_j^k}{\varepsilon}\right) \exp\left(\frac{\|C\|_\infty}{\varepsilon}\right) |w - w'| a_i b_j \\ &\leq (\|\tilde{C}\|_\infty^2 / \varepsilon) \exp(6\|C\|_\infty / \varepsilon) |w - w'|, \end{aligned}$$

where $\tilde{C}_{ij} = \|x_i - y_j\|_p^p - |t_i - s_j|^p$. The first inequality uses the inequality in (22), and the definition of $\|\tilde{C}\|_\infty = \max\{|\tilde{C}_{ij}| : i \in [m], j \in [n]\}$. The second inequality invokes the bounds from lemma 3.1.

D Proof of lemma 3.3

In this proof, we shall use the strong convexity of the exponential function in a bounded region. Given $M > 0$, we have that for any $(a, b) \in [-M, M] \times [-M, M]$,

$$e^b - e^a - e^a(b - a) \geq e^{-M}(b - a)^2/2, \quad (23)$$

Let $\Delta_u F = F(u^k, v^k, w^k) - F(u^{k+1}, v^k, w^k)$, $\Delta_v F = F(u^{k+1}, v^k, w^k) - F(u^{k+1}, v^{k+1}, w^k)$ and $\Delta_w F = F(u^{k+1}, v^{k+1}, w^k) - F(u^{k+1}, v^{k+1}, w^{k+1})$. We have

$$F(u^k, v^k, w^k) - F(u^{k+1}, v^{k+1}, w^{k+1}) = \Delta_u F + \Delta_v F + \Delta_w F.$$

Next we will evaluate each of these terms separately.

$$\Delta_u F = \varepsilon \sum_{i=1}^m \sum_{j=1}^n \left(e^{\frac{u_i^k}{\varepsilon}} - e^{\frac{u_i^{k+1}}{\varepsilon}} \right) e^{\frac{v_j^k}{\varepsilon}} e^{\frac{-c_{ij}(w^k)}{\varepsilon}} a_i b_j \quad (24)$$

$$\geq \sum_{i=1}^m \sum_{j=1}^n (u_i^k - u_i^{k+1}) e^{\frac{u_i^{k+1}}{\varepsilon}} e^{\frac{v_j^k}{\varepsilon}} e^{\frac{-c_{ij}(w^k)}{\varepsilon}} a_i b_j + \kappa \sum_{i=1}^m (u_i^k - u_i^{k+1})^2 a_i \quad (25)$$

$$= e^{\frac{\lambda^k}{\varepsilon}} \sum_{i=1}^m (u_i^k - u_i^{k+1}) a_i + \kappa \sum_{i=1}^m (u_i^k - u_i^{k+1})^2 a_i \quad (26)$$

$$= \kappa \|u^k - u^{k+1}\|_{L^2(\alpha)}^2, \quad (27)$$

where $\kappa := \frac{e^{-6\|C\|_\infty}}{2\varepsilon}$. In the above, inequality (25) is obtained by first applying the local strong convexity (23) with $M = 2\|C\|_\infty / \varepsilon$ and then applying the bound $\exp\left(\frac{v_j^k - c_{ij}(w^k)}{\varepsilon}\right) \geq \exp\left(-\frac{4\|C\|_\infty}{\varepsilon}\right)$ to the second term. The equality (26) is obtained by substituting the update expression of u_i^{k+1} into $\exp\left(\frac{u_i^{k+1}}{\varepsilon}\right)$ in the first term of (25). The equality (27) comes from the fact that $(u^k - u^{k+1})^\top a = 0$ due to the normalization.

Although v^k has no normalization property, following analogous arguments, we still obtain

$$\Delta_v F \geq \kappa \|v^k - v^{k+1}\|_{L^2(\beta)}^2.$$

In order to evaluate the last term, first we recall the following basic property of the projection operator onto a closed convex set $D \subset \mathbf{R}$:

$$\langle \mathbf{y} - P_D(\mathbf{y}), \mathbf{x} - P_D(\mathbf{y}) \rangle \leq 0 \quad \text{for any } \mathbf{x} \in D, \mathbf{y} \in \mathbf{R}. \quad (28)$$

Applying this property with $\mathbf{x} = w^k, \mathbf{y} = w^k - \eta \nabla_w F(u^{k+1}, v^{k+1}, w^k)$, we get

$$\langle \nabla_w F(u^{k+1}, v^{k+1}, w^k), w^k - w^{k+1} \rangle \geq \frac{1}{\eta} |w^k - w^{k+1}|^2. \quad (29)$$

Combining $\eta = (\varepsilon / \|\tilde{C}\|_\infty^2) \exp(-6\|C\|_\infty / \varepsilon)$ with lemma 3.2, we obtain the Lipschitz continuity with constant $1/\eta$ of $\nabla_w F(u^k, v^k, w)$ over the compact set $[0, 1]$ for all $k \geq 1$. Therefore, by invoking the descent lemma [3], we have

$$\Delta_w F \geq -\langle \nabla_w F(u^{k+1}, v^{k+1}, w^k), w^{k+1} - w^k \rangle - \frac{1}{2\eta} |w^k - w^{k+1}|^2.$$

Combining this with (29) implies that

$$\Delta_w F \geq \frac{1}{2\eta} |w^k - w^{k+1}|^2 = \tau |w^k - w^{k+1}|^2,$$

where $\tau = \|\tilde{C}\|_\infty^2 \exp(6\|C\|_\infty / \varepsilon) / 2\varepsilon$.

E Proof of lemma 3.5

By Theorem 3.4 and the equivalence of $\|\cdot\|_2$ and $\|\cdot\|_\infty$, we have $\inf_{\xi \in \tilde{\mathcal{S}}} \|\xi^k - \xi\|_\infty \rightarrow 0$ as $k \rightarrow \infty$. By the definition of infimum, for each $k \geq 1$, we can choose $\xi_k^* \in \tilde{\mathcal{S}}$ such that $\|\xi^k - \xi_k^*\|_\infty \leq 1/k + \inf_{\xi \in \tilde{\mathcal{S}}} \|\xi^k - \xi\|_\infty$. Take the limit $k \rightarrow \infty$, we deduce $\|\xi^k - \xi_k^*\|_\infty \rightarrow 0$. Next, we consider

$$\|\xi_k^*\|_\infty \leq \|\xi^k - \xi_k^*\|_\infty + \|\xi^k\|_\infty \leq \|\xi^k - \xi_k^*\|_\infty + \max\{1, 3\|C\|_\infty\}, \quad (30)$$

where the first inequality uses the triangle inequality and the second inequality uses the bounds of u^k, v^k, w^k from Lemma 3.1. Since $\{\xi^k - \xi_k^*\}$ converges, it is bounded. Therefore, from (30), we have that $\{\xi_k^*\}$ is bounded. Moreover, $\tilde{\mathcal{S}}$ is closed, as it is the preimage of a closed set. Hence, there exists a subsequence $\{\xi_{k_i}^*\}$ which converges to $\xi^* = (u^*, v^*, w^*) \in \tilde{\mathcal{S}}$. Using (30), we have

$$\|u_{k_i}^*\|_\infty \leq \|u^{k_i} - u_{k_i}^*\|_\infty + \|u^{k_i}\|_\infty \leq \|u^{k_i} - u_{k_i}^*\|_\infty + 2\|C\|_\infty.$$

Taking $i \rightarrow \infty$ on both sides, we obtain $\|u^*\| \leq 2\|C\|_\infty$. Similarly, we can derive that $\|v^*\|_\infty \leq 3\|C\|_\infty$.

F Proof of theorem 3.6

The proof proceeds in four steps. **Step 1** upper bounds the optimality gap $F(\xi^{k+1}) - F^*$ by the norm of the gradient difference. **Step 2** exploits the locally Lipschitz property of the exponential function to bound the norm of the gradient difference by the successive changes of the iterates. **Step 3** applies the sufficient descent property to bound the successive changes of the iterates by the successive decreases in the function value. **Step 4** utilizes the inequality established from Step 3 and [25, Theorem 3.1(1)] to immediately obtain the sublinear convergence rate of (17).

Step 1: let $\xi^* = (u^*, v^*, w^*)$ be an optimal solution of (16) satisfying $\|u^*\|_\infty \leq 2\|C\|_\infty$, $\|v^*\|_\infty \leq 3\|C\|_\infty$, its existence follows from Lemma 3.5. Denote $\xi^{k+1/3} = (u^{k+1}, v^k, w^k)$ and $\xi^{k+2/3} = (u^{k+1}, v^{k+1}, w^k)$. By the convexity of $F(\cdot)$, we have

$$\begin{aligned} F(\xi^{k+1}) - F^* &\leq \langle \nabla F(\xi^{k+1}), \xi^{k+1} - \xi^* \rangle \\ &= \langle \nabla_u F(\xi^{k+1}), u^{k+1} - u^* \rangle + \langle \nabla_v F(\xi^{k+1}), v^{k+1} - v^* \rangle \\ &\quad + \nabla_w F(\xi^{k+1})(w^{k+1} - w^*). \end{aligned} \quad (31)$$

Next, we bound the terms on the RHS of (31) separately. First, we have that

$$\begin{aligned} \langle \nabla_u F(\xi^{k+1}), u^{k+1} - u^* \rangle &= \langle \nabla_u F(\xi^{k+1}) - \nabla_u F(\xi^{k+1/3}) + \nabla_u F(\xi^{k+1/3}), u^{k+1} - u^* \rangle \\ &\leq \langle \nabla_u F(\xi^{k+1}) - \nabla_u F(\xi^{k+1/3}), u^{k+1} - u^* \rangle \\ &\leq \|\nabla_u F(\xi^{k+1}) - \nabla_u F(\xi^{k+1/3})\|_2 \|u^{k+1} - u^*\|_2 \\ &\leq \sqrt{m} \|\nabla_u F(\xi^{k+1}) - \nabla_u F(\xi^{k+1/3})\|_2 \|u^{k+1} - u^*\|_\infty \\ &\leq 4\sqrt{m} \|C\|_\infty \|\nabla_u F(\xi^{k+1}) - \nabla_u F(\xi^{k+1/3})\|_2. \end{aligned}$$

Here the first inequality is established by using the first-order optimality condition for u^{k+1} with respect to φ_u^k , which gives $\langle \nabla_u F(\xi^{k+1/3}), u^{k+1} - u^* \rangle < 0$. The second inequality leverages the Cauchy–Schwarz inequality, the third follows from the equivalence of norms, and the last relies on the triangle inequality and the bounds of $\|u^k\|_\infty$ and $\|u^*\|_\infty$.

Similarly, utilizing the optimality of v^{k+1} , and w^{k+1} of the upper bound functions $\varphi_v^k(v) = F(u^{k+1}, v, w^k)$ and $\varphi_w^k(w) = F(\xi^{k+2/3}) + \nabla_w F(\xi^{k+2/3})(w - w^k) + \frac{1}{2\eta}(w - w^k)^2$, we obtain

$$\begin{aligned} \langle \nabla_v F(\xi^{k+1}), v^{k+1} - v^* \rangle &\leq 6\sqrt{n} \|C\|_\infty \|\nabla_v F(\xi^{k+1}) - \nabla_v F(\xi^{k+2/3})\|_2, \\ \nabla_w F(\xi^{k+1})(w^{k+1} - w^*) &\leq |\nabla_w F(\xi^{k+1}) - \nabla \varphi_w^k(w^{k+1})|. \end{aligned}$$

Denote $\mathbf{D}_u^k = \nabla_u F(\xi^{k+1}) - \nabla_u F(\xi^{k+1/3})$, $\mathbf{D}_v^k = \nabla_v F(\xi^{k+1}) - \nabla_v F(\xi^{k+2/3})$, and $\mathbf{D}_w^k = \nabla_w F(\xi^{k+1}) - \nabla \varphi_w^k(w^{k+1})$, it follows from (31) and the above inequalities that

$$F(\xi^{k+1}) - F^* \leq 4\sqrt{m} \|C\|_\infty \|\mathbf{D}_u^k\|_2 + 6\sqrt{n} \|C\|_\infty \|\mathbf{D}_v^k\|_2 + |\mathbf{D}_w^k|,$$

which by Cauchy–Schwarz inequality implies

$$(F(\xi^{k+1}) - F^*)^2 \leq 3(16m \|C\|_\infty^2 \|\mathbf{D}_u^k\|_2^2 + 36n \|C\|_\infty^2 \|\mathbf{D}_v^k\|_2^2 + (\mathbf{D}_w^k)^2). \quad (32)$$

Step 2: we next proceed to bound $\|\mathbf{D}_u^k\|_2^2$ by component-wise analysis. Specifically, we

examine each entry $\mathbf{D}_{u_i}^k$:

$$\begin{aligned}
(\mathbf{D}_{u_i}^k)^2 &= \left[\sum_{j=1}^n \exp\left(\frac{u_i^{k+1}}{\varepsilon}\right) \left(\exp\left(\frac{v_j^{k+1} - C_{ij}(w^{k+1})}{\varepsilon}\right) - \exp\left(\frac{v_j^k - C_{ij}(w^k)}{\varepsilon}\right) \right) a_i b_j \right]^2 \\
&\leq a_i^2 \sum_{j=1}^n \exp\left(\frac{2u_i^{k+1}}{\varepsilon}\right) \left(\exp\left(\frac{v_j^{k+1} - C_{ij}(w^{k+1})}{\varepsilon}\right) - \exp\left(\frac{v_j^k - C_{ij}(w^k)}{\varepsilon}\right) \right)^2 b_j \\
&\leq \frac{a_i^2}{\varepsilon^2} \exp\left(\frac{12\|C\|_\infty}{\varepsilon}\right) \left(\sum_{j=1}^n (v_j^{k+1} - v_j^k + \tilde{C}_{ij}(w^{k+1} - w^k))^2 b_j \right) \\
&\leq \frac{2a_i^2}{\varepsilon^2} \exp\left(\frac{12\|C\|_\infty}{\varepsilon}\right) \left(\sum_{j=1}^n (v_j^{k+1} - v_j^k)^2 b_j + \tilde{C}_{ij}^2 (w^{k+1} - w^k)^2 b_j \right) \\
&\leq \frac{2a_i^2}{\varepsilon^2} \exp\left(\frac{12\|C\|_\infty}{\varepsilon}\right) \left(\|v^{k+1} - v^k\|_{L^2(b)}^2 + \|\tilde{C}\|_\infty^2 (w^{k+1} - w^k)^2 \right),
\end{aligned}$$

where $\tilde{C}_{ij} = \|x_i - y_j\|_p^p - |t_i - s_j|^p$. The first inequality uses the Cauchy-Schwarz inequality and the property $\left(\sum_{j=1}^n b_j\right) = 1$, the second leverages (22) and the bounds from lemma 3.1, the third again exploits the Cauchy-Schwarz inequality. Finally, the last inequality uses the definitions of $\|\cdot\|_{L(b)}$ and $\|\tilde{C}\|_\infty$. Given that $(\sum_{i=1}^m a_i^2) \leq 1$, we deduce that

$$\|\mathbf{D}_u^k\|_2^2 \leq \frac{2}{\varepsilon^2} \exp\left(\frac{12\|C\|_\infty}{\varepsilon}\right) \left(\|v^{k+1} - v^k\|_{L^2(b)}^2 + \|\tilde{C}\|_\infty^2 (w^{k+1} - w^k)^2 \right). \quad (33)$$

Using similar arguments, we obtain that

$$\|\mathbf{D}_v^k\|_2^2 \leq \frac{\|\tilde{C}\|_\infty^2}{\varepsilon^2} \exp\left(\frac{12\|C\|_\infty}{\varepsilon}\right) (w^{k+1} - w^k)^2. \quad (34)$$

To complete Step 2, we evaluate

$$\begin{aligned}
|\mathbf{D}_w^k| &= |\nabla F_w(\xi^{k+1}) - \nabla F_w(\xi^{k+2/3}) - (1/\eta)(w^{k+1} - w^k)| \\
&\leq |\nabla F_w(\xi^{k+1}) - \nabla F_w(\xi^{k+2/3})| + \frac{\|\tilde{C}\|_\infty^2}{\varepsilon} \exp\left(\frac{6\|C\|_\infty}{\varepsilon}\right) |w^{k+1} - w^k| \\
&\leq \sum_{i=1}^m \sum_{j=1}^n \|\tilde{C}\|_\infty \exp\left(\frac{5\|C\|_\infty}{\varepsilon}\right) \left| \exp\left(\frac{-C_{ij}(w^{k+1})}{\varepsilon}\right) - \exp\left(\frac{-C_{ij}(w^k)}{\varepsilon}\right) \right| a_i b_j \\
&\quad + (\|\tilde{C}\|_\infty^2 / \varepsilon) \exp\left(\frac{6\|C\|_\infty}{\varepsilon}\right) |w^{k+1} - w^k| \\
&\leq (2\|\tilde{C}\|_\infty^2 / \varepsilon) \exp\left(\frac{6\|C\|_\infty}{\varepsilon}\right) |w^{k+1} - w^k| \\
&\leq (2\|\tilde{C}\|_\infty \|C\|_\infty / \varepsilon) \exp\left(\frac{6\|C\|_\infty}{\varepsilon}\right) |w^{k+1} - w^k|,
\end{aligned} \quad (35)$$

where the first inequality follows from the triangle inequality and the formula of the stepsize η , the second uses the triangle inequality of the absolute value and the bounds of $u^{k+1}, v^{k+1}, \tilde{C}_{ij}$, the third leverages (22), and the last uses the fact that $\|\tilde{C}\|_\infty \leq \|C(1)\|_\infty \leq \|C\|_\infty$.

Now, substitute (33), (34), (35) into (32), we arrive at

$$\begin{aligned}
(F(\xi^{k+1}) - F^*)^2 &\leq 96m\rho \left(\|v^{k+1} - v^k\|_{L^2(b)}^2 + \|\tilde{C}\|_\infty^2 (w^{k+1} - w^k)^2 \right) \\
&\quad + \rho \left(108n\|\tilde{C}\|_\infty^2 (w^{k+1} - w^k)^2 + 12\|\tilde{C}\|_\infty^2 (w^{k+1} - w^k)^2 \right) \\
&\leq \rho(96m + 108n + 12) \left(\|v^{k+1} - v^k\|_{L^2(b)}^2 + \|\tilde{C}\|_\infty^2 (w^{k+1} - w^k)^2 \right),
\end{aligned}$$

where $\rho = \frac{\|C\|_\infty^2}{\varepsilon^2} \exp\left(\frac{12\|C\|_\infty}{\varepsilon}\right)$.

Step 3: By using the sufficient descent property (Lemma 3.3) to upper bound the RHS of the above inequality, we obtain

$$(F(\xi^{k+1}) - F^*)^2 \leq \rho_1 (F(\xi^k) - F(\xi^{k+1})), \quad (36)$$

where $\rho_1 = (192m + 216n + 24) \frac{\|C\|_\infty^2}{\varepsilon} \exp(\frac{18\|C\|_\infty}{\varepsilon})$.

Step 4: From the analysis presented in [25, Theorem 3.1(1)] and the inequality (36), the proof is completed.

G TiOT as a Linear Program

Following similar steps as in Section 3, we can rewrite the TiOT problem as

$$\min \left\{ q^\top z \mid Hz \leq r, w \in [0, 1], z = [u; v; w] \in \mathbb{R}^{m+n+1} \right\} \quad (37)$$

where $q = [a; b; 0] \in \mathbb{R}^{m+n+1}$, the constraint matrix is

$$H \in \mathbb{R}^{mn \times (m+n+1)}, \quad H_{i+(j-1)n,:} = (-e_i^\top, -e_j^\top, (t_i - s_j)^2 - \|x_i - y_j\|^2),$$

and $r_{i+(j-1)n} = (t_i - s_j)^2$, for $i \in [m]$ and $j \in [n]$.

H Additional experiments on time series classification

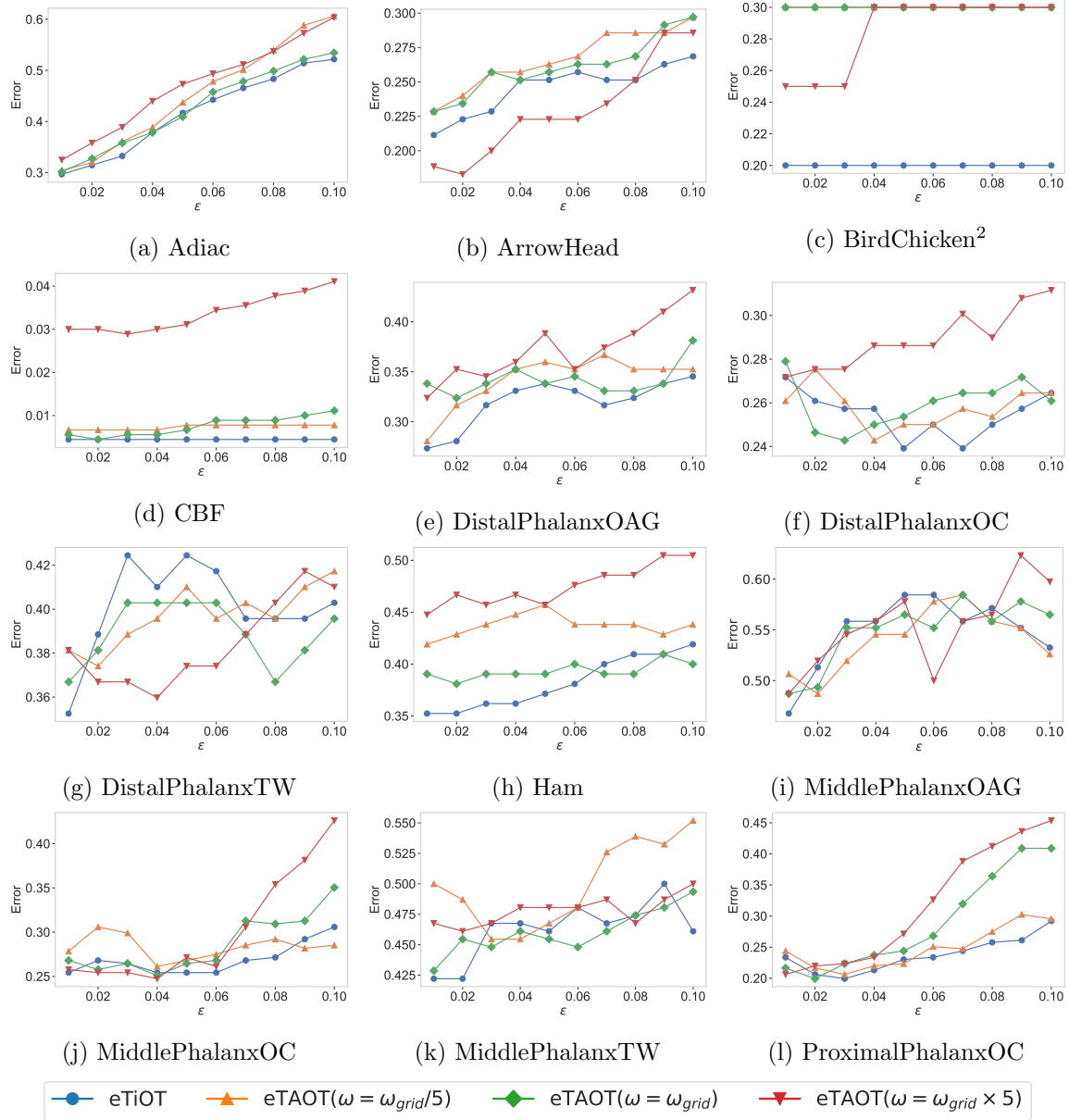


Figure 5: Classification error of 1NN algorithm with $\epsilon = 0.01, \dots, 0.1$.

²For the BirdChicken dataset, due to the small test set, eTAOT($w = w_{\text{grid}}/5$) and eTAOT($w = w_{\text{grid}}$) produce identical errors (0.30).